

D and D^* mesons in isospin asymmetric nuclear medium

Anshu Gautam,^{*} Dhananjay Singh,[†] Navpreet Kaur,[‡] Satyajit
Puhan,[§] Suneel Dutt,[¶] Harleen Dahiya,^{**} and Arvind Kumar^{††}

*Department of Physics, Dr. B.R. Ambedkar National
Institute of Technology, Jalandhar, 144008, India*

(Dated: June 11, 2025)

Abstract

We investigate the properties of pseudoscalar D and vector D^* mesons in an isospin asymmetric nuclear medium using a hybrid approach that integrates the light-front quark model with the chiral SU(3) quark mean field model. The influence of isospin asymmetric nuclear medium is examined by utilizing the in-medium quark masses derived from the chiral SU(3) quark mean field model as an input in the light-front quark model to study the medium modification of D mesons. We examine the impact of isospin asymmetry and baryon density at zero and finite temperature on the effective masses, weak decay constants, and distribution amplitudes of the pseudoscalar mesons D^0 , D^+ , D_s , and the vector mesons D^{0*} , D^{+*} , and D_s^* . Our results indicate significant medium-induced changes for pseudoscalar D and vector D^* mesons having u/d as one of their constituent quarks, while a comparatively reduced effect is observed for mesons containing a strange quark. In contrast to temperature and isospin asymmetry, changes in the baryon density of the nuclear medium have a larger effect on different properties of D and D^* mesons.

Keywords: Nuclear medium, isospin asymmetry, weak decay constants, distribution amplitudes (DAs), quark model.

I. INTRODUCTION

Investigating the properties and internal structure of hadrons in the nuclear medium is among the most active areas of research in hadronic physics, essential for understanding strongly interacting matter under extreme conditions. Through the deep inelastic scattering (DIS) experiments, the European Muon Collaboration (EMC) observed that the structure function of nucleons bound inside the nuclei is different compared to free space [1]. This finding suggests that the interaction between nucleons and their surrounding medium alters the internal structure of the nucleus. Moreover, the medium modification of hadron properties may relate to the partial restoration of chiral symmetry. Experimental evidence supporting this phenomenon has been observed in deeply bound pionic atoms [2], low-energy pion-nucleus scattering [3], and di-pion production in hadron and photon-nucleus interactions [4, 5], all highlighting substantial modifications to pion properties

* gautamanshu681@gmail.com

† snaks16aug@gmail.com

‡ knavpreet.hep@gmail.com

§ puhansatyajit@gmail.com

¶ dutts@nitj.ac.in

** dahiyah@nitj.ac.in

†† kumara@nitj.ac.in

in the nuclear environment. Specifically, the studies of deeply bound pionic atoms [2] and pion-nucleus scattering [3] have shown a reduction in the pion decay constant, indicating that pions behave differently when bound within a nuclear medium.

Investigating how hadron properties are affected in nuclear medium at various temperatures and densities is crucial in high-energy physics as it provides insight into the behavior of strongly interacting matter under extreme conditions. Different experimental facilities, such as the proton-antiproton annihilation (PANDA) of GSI, Germany, focus on investigations related to hadron spectroscopy and the modifications of mass and width within the charm region [6]. The Japan proton accelerator research complex (J-PARC) in Japan [7, 8] is designed to undertake measurements of hadrons, fluctuations in conserved quantities, dileptons, and multi-strange hypernuclei by utilizing the world's most intense heavy-ion beam to address the physics of high-density matter [9]. In parallel, the compressed baryonic matter experiment (CBM) at GSI, Germany [10] and the nuclotron-based ion collider facility (NICA) in Dubna, Russia [11, 12] aim to probe the nonperturbative aspects of quantum chromodynamics (QCD) at finite baryon density [13].

Motivated by these experimental developments, various theoretical approaches have been employed in the past to study the in-medium properties of hadrons such as the two-part model for the EMC effect based on light-front holographic QCD (LFHQCD) [14], Nambu–Jona-Lasinio (NJL) model combined with the quark meson coupling (QMC) model [15], the Dyson-Schwinger equation (DSE) based approach [16] and the hybrid light front-quark meson coupling (LF-QMC) [17, 18]. Additionally, the impact of nuclear medium on the properties of pions and kaons is studied within the light cone quark model (LCQM) and chiral SU(3) quark mean field (CQMF) model [19–22]. The properties of B mesons have also been investigated recently using the combined approach of LCQM and CQMF models [23]. In Refs. [15, 24, 25], studies demonstrate how hadrons' internal structure and properties are modified in a nuclear medium due to changes in the underlying quark condensates and meson-baryon interactions. Nonetheless, extensive research has been conducted on the medium modification of mesons in both symmetric and asymmetric nuclear medium. In the present work, we are primarily concerned with how the properties of pseudoscalar D mesons (D^0, D^+, D_s) and vector D^* mesons (D^{0*}, D^{+*}, D_s^*), such as their masses, weak decay constants, and distribution amplitudes (DAs) are affected in a nuclear medium.

The interest in the properties of both open and hidden charmed mesons was sparked over two decades ago, mainly due to the investigation of relativistic nucleus-nucleus collisions. A key reason for this was charmonium suppression [26], proposed as an indicator of quark gluon plasma

(QGP) formation. Following the observation of J/ψ suppression at super proton synchrotron (SPS) energies by the NA50 collaboration [27], the medium modifications of D mesons have become particularly significant, as it provides crucial insights into the behavior of heavy quarks within dense nuclear matter, which is vital for understanding the dynamics of QGP and the hadronization process in high-energy collisions. One of the consequences of in-medium interactions is that the attractive potential experienced by D mesons in the nuclear medium may also lead to the formation of D -mesic [28] and J/ψ -mesic nuclei [29, 30]. To probe these medium effects, the spectral density of D mesons has been analyzed using a self-consistent coupled channel approach [31–33], indicating that in-medium modifications predominantly affect the meson width, contrary to earlier expectations about the mass shift, particularly in the context of nucleus-nucleus collisions at FAIR (GSI) [34]. A negative mass shift of ~ 50 MeV for the D meson was observed in the symmetric nuclear matter by employing the QCD sum rule [35]. Moreover, a comparable reduction in the mass of around 60 MeV at nuclear saturation density was obtained in the calculations using the QMC model [36]. The chiral SU(3) hadronic mean field model has been used to explore the in-medium masses of D and \bar{D} mesons in nuclear and strange medium [37, 38]. The interaction of D mesons with the nucleons and the scalar mesons in a magnetized asymmetric nuclear medium has been studied using an effective hadronic model [39]. The integration of the chiral SU(3) hadronic framework with QCD sum rules has been used to explore the mass shifts and decay constants of both pseudoscalar and scalar D mesons in a hot magnetized asymmetric nuclear medium [40]. Furthermore, this combined approach has also been applied to evaluate the in-medium masses and decay constants of pseudoscalar, scalar, vector, and axial-vector D mesons in strange hadronic environments [41–44].

In the present manuscript, we investigate the properties of pseudoscalar D and vector D^* mesons under varying conditions of isospin asymmetry and temperature of the dense nuclear medium. The modification of meson masses in a medium is primarily governed by the interaction of light quarks with the nuclear medium, as they respond sensitively to changes in quark condensates associated with chiral symmetry breaking [15, 45]. In contrast, heavy quarks are only slightly influenced due to their large masses. The weak decay constant represents the meson’s decay amplitude via weak interactions and serves as a key indicator of chiral symmetry breaking in dense matter [46, 47]. Furthermore, the DAs of mesons are crucial for analyzing SU(3) symmetry breaking effects and play an important role in understanding hard exclusive QCD processes involving large momentum transfers [48, 49]. In this study, we employ a hybrid framework wherein meson properties are

evaluated using the light-front quark model (LFQM), while in-medium quark masses are supplied by the chiral SU(3) quark mean field (CQMF) model. The LFQM framework provides an effective nonperturbative method that uses quantization at equal light-front time ($x^+ = t + z$) and evolves the system via the light-front Hamiltonian P^- [50, 51]. The model uses a Gaussian wave function as the trial state for applying the variational principle to the QCD motivated Hamiltonian that incorporates the quark potential, which effectively captures the interaction between quark and antiquark within the meson. While the nuclear medium notably impacts lighter quarks more than heavier ones, isospin asymmetric matter relevant to both neutron stars and heavy-ion collisions introduces additional complexity. We include the effects of isospin asymmetry via in-medium quark masses computed using the CQMF model. In the CQMF model, quarks are confined within baryons by means of a confining potential and engage in interactions through the exchange of scalar (σ, ζ, δ) and vector (ω, ρ) fields.

The paper is organized as follows: In Sec. II A, we present the CQMF model employed for computing the in-medium quark masses. Sec. II B introduces the effective Hamiltonian and light front wave function (LFWF) adopted in the present approach. Results of the present work on the in-medium properties of pseudoscalar and vector D mesons are presented in Sec. III, and lastly in Sec. IV, we summarize our findings.

II. METHODOLOGY

A. Chiral SU(3) quark mean field model

The CQMF model is used to evaluate effective quark masses within an isospin asymmetric nuclear medium, which serve as input to investigate the medium-modified properties of D mesons. The model treats quarks and mesons as fundamental degrees of freedom and incorporates important low-energy features of QCD, particularly the spontaneous and explicit breaking of chiral symmetry [52]. As discussed earlier, quarks are confined within baryons through an effective potential and acquire their masses via interactions with the scalar-isoscalar fields σ and ζ , the scalar-isovector field δ , and the vector-isoscalar ω along with the vector-isovector field ρ . The trace anomaly property of QCD is accounted for by the inclusion of scalar dilation field χ [53, 54], while the δ and ρ fields introduce isospin asymmetry into the medium [55].

The thermodynamic potential for isospin asymmetric nuclear matter at finite temperature and

density is expressed as

$$\Omega = -\frac{k_B T}{(2\pi)^3} \sum_i \gamma_i \int_0^\infty d^3 k \left[\ln \left(1 + e^{-\left(\frac{E_i^*(k) - \nu_i^*}{k_B T} \right)} \right) + \ln \left(1 + e^{-\left(\frac{E_i^*(k) + \nu_i^*}{k_B T} \right)} \right) \right] - \mathcal{L}_M - \mathcal{V}_{\text{vac}}, \quad (1)$$

where the summation over nucleons in the medium is represented by $i = p/n$ and the degeneracy factor $\gamma_i = 2$ accounts for two spin states of each nucleon. The effective energy $E_i^*(k)$ and the effective chemical potential ν_i^* of the baryon are expressed as

$$E_i^* = \sqrt{M_i^{*2} + k^2}, \quad (2)$$

$$\nu_i^* = \nu_i - g_\omega^i \omega - g_\rho^i I^3 \rho. \quad (3)$$

In above, M_i^* is the effective mass of the baryon and ν_i is the free chemical potential. To obtain the density and temperature dependent values of scalar, vector, and dilaton fields, the thermodynamic potential is minimized as

$$\frac{\partial \Omega}{\partial \sigma} = \frac{\partial \Omega}{\partial \zeta} = \frac{\partial \Omega}{\partial \delta} = \frac{\partial \Omega}{\partial \chi} = \frac{\partial \Omega}{\partial \omega} = \frac{\partial \Omega}{\partial \rho} = 0. \quad (4)$$

This yields a set of nonlinear equations, which are solved for different values of baryon density, temperature, and isospin asymmetry. The effect of isospin asymmetry is quantified by the parameter $\eta = -\frac{\sum_i I_{3i} \rho_i}{\rho_B}$, where I_{3i} represents the 3rd component of isospin quantum number and ρ_B denotes the total baryon density of the medium. The effective Lagrangian density which encapsulates the interactions within the CQMF model is given by [52]

$$\mathcal{L}_{\text{eff}} = \mathcal{L}_{q0} + \mathcal{L}_{qm} + \mathcal{L}_{\Sigma\Sigma} + \mathcal{L}_{VV} + \mathcal{L}_{\chi SB} + \mathcal{L}_{\Delta m} + \mathcal{L}_c. \quad (5)$$

In the above, \mathcal{L}_{q0} denotes the kinetic term and \mathcal{L}_{qm} represents the quark-meson interaction term, including quark interactions with both spin-0 and spin-1 mesons [52, 56, 57]. The expressions for \mathcal{L}_{q0} and \mathcal{L}_{qm} are written as

$$\mathcal{L}_{q0} = \bar{q} i \gamma^\mu \partial_\mu q, \quad (6)$$

and

$$\begin{aligned}
\mathcal{L}_{qm} &= g_s (\bar{\Psi}_L M \Psi_R + \bar{\Psi}_R M^\dagger \Psi_L) - g_v (\bar{\Psi}_L \gamma^\mu l_\mu \Psi_L + \bar{\Psi}_R \gamma^\mu r_\mu \Psi_R) \\
&= \frac{g_s}{\sqrt{2}} \bar{\Psi} \left(\sum_{a=0}^8 s_a \lambda_a + i \gamma^5 \sum_{a=0}^8 p_a \lambda_a \right) \Psi \\
&\quad - \frac{g_v}{2\sqrt{2}} \bar{\Psi} \left(\gamma^\mu \sum_{a=0}^8 v_a^\mu \lambda_a - \gamma^\mu \gamma^5 \sum_{a=0}^8 a_a^\mu \lambda_a \right) \Psi,
\end{aligned} \tag{7}$$

respectively. Here, $q = \begin{pmatrix} u \\ d \end{pmatrix}$ and parameters g_s and g_v describe couplings of quark with scalar and vector meson fields. From Eq. (5), the chiral invariant self-interaction term for scalar mesons $\mathcal{L}_{\Sigma\Sigma}$ is expressed as

$$\begin{aligned}
\mathcal{L}_{\Sigma\Sigma} &= -\frac{1}{2} k_0 \chi^2 (\sigma^2 + \zeta^2 + \delta^2) + k_1 (\sigma^2 + \zeta^2 + \delta^2)^2 + k_2 \left(\frac{\sigma^4}{2} + \frac{\delta^4}{2} + 3\sigma^2 \delta^2 + \zeta^4 \right) \\
&\quad + k_3 \chi (\sigma^2 - \delta^2) \zeta - k_4 \chi^4 - \frac{1}{4} \chi^4 \ln \frac{\chi^4}{\chi_0^4} + \frac{\xi}{3} \chi^4 \ln \left(\left(\frac{(\sigma^2 - \delta^2) \zeta}{\sigma_0^2 \zeta_0} \right) \left(\frac{\chi^3}{\chi_0^3} \right) \right).
\end{aligned} \tag{8}$$

In the above, the last two logarithmic terms are included to ensure the trace of the energy-momentum tensor is proportional to the fourth power of the dilaton field χ . For vector mesons, the self-interaction term \mathcal{L}_{VV} is given by

$$\mathcal{L}_{VV} = \frac{1}{2} \frac{\chi^2}{\chi_0^2} (m_\omega^2 \omega^2 + m_\rho^2 \rho^2) + g_4 (\omega^4 + 6\omega^2 \rho^2 + \rho^4). \tag{9}$$

To incorporate the non-zero masses of pseudoscalar mesons, the explicit symmetry-breaking term $\mathcal{L}_{\chi SB}$ is introduced in Eq (5) as [54, 58]

$$\mathcal{L}_{\chi SB} = -\frac{\chi^2}{\chi_0^2} \left[m_\pi^2 f_\pi \sigma + \left(\sqrt{2} m_K^2 f_K - \frac{m_\pi^2}{\sqrt{2}} f_\pi \right) \zeta \right]. \tag{10}$$

Finally, to represent quark confinement within baryons, the confining potential term \mathcal{L}_c is written as

$$\mathcal{L}_c = -\bar{\psi} \chi_c \psi. \tag{11}$$

In the presence of meson mean fields, the Dirac equation for a quark field Ψ_{qi} becomes

$$\left[-i\alpha \cdot \nabla + \chi_c(r) + \beta m_q^*\right] \Psi_{qi} = e_q^* \Psi_{qi}, \quad (12)$$

where the subscript q represents the quarks within a baryon of type i (where $i=n, p$) and α, β denote the standard Dirac matrices. The effective quark mass m_q^* and energy e_q^* are expressed in terms of relevant coupling constants, and the scalar and vector meson fields as [59]

$$m_q^* = -g_\sigma^q \sigma - g_\zeta^q \zeta - g_\delta^q I^{3q} \delta + \Delta m, \quad (13)$$

and

$$e_q^* = e_q - g_\omega^q \omega - g_\rho^q I^{3q} \rho. \quad (14)$$

The Lagrangian density $\mathcal{L}_{\Delta m} = -(\Delta m) \bar{\psi} S_1 \psi$ is incorporated through an explicit symmetry breaking term to attain a realistic value for the strange quark mass m_s , where S_1 is the strange quark matrix operator and is defined as $S_1 = \frac{1}{3} (I - \lambda_8 \sqrt{3}) = \text{diag}(0, 0, 1)$ [52, 58]. The value of Δm for the u and d quarks is zero, while for the s quark $\Delta m = 77$ MeV. The various parameters and coupling constants used in our calculations are listed in Table I.

The in-medium spurious center-of-mass momentum $\langle p_{i\text{cm}}^{*2} \rangle$ [60, 61] and the effective energy of constituent quarks e_q^* are related to the effective mass of the i^{th} baryon through the relation

$$M_i^* = \sqrt{\left(\sum_q n_{qi} e_q^* + E_{i\text{spin}}\right)^2 - \langle p_{i\text{cm}}^{*2} \rangle}. \quad (15)$$

Here, n_{qi} denotes the number of quarks of type q within the i^{th} baryon. Additionally, the in-medium spurious center-of-mass correction $\langle p_{i\text{cm}}^{*2} \rangle$ is given by

$$\langle p_{i\text{cm}}^{*2} \rangle = \sum_q \frac{(11e_q^* + m_q^*)}{6(3e_q^* + m_q^*)} (e_q^{*2} - m_q^{*2}). \quad (16)$$

B. Light-front quark model

This section describes the fundamental idea of LFQM, which includes the effective Hamiltonian and the light front wave function (LFWF). To preserve compliance with the group structure satisfying the Poincaré algebraic commutation relations, the interactions are incorporated into the meson mass operator [62]. The model is based on the idea of using a radial wave function as a trial state for the QCD motivated effective Hamiltonian with a linear confinement potential [63], which determines the mass eigenvalue by employing the variational principle framework.

The meson bound system at rest satisfying the eigenvalue equation of the QCD inspired effective Hamiltonian is described as [48, 64, 65],

$$(H_0 + V_{q\bar{q}}) |\Psi_{q\bar{q}}\rangle = M_{q\bar{q}}^* |\Psi_{q\bar{q}}\rangle, \quad (17)$$

where $\Psi_{q\bar{q}}$ and $M_{q\bar{q}}$ are the eigenfunction and mass eigenvalue of the meson, respectively. The relativistic kinetic energy of the quark and antiquark is given by

$$H_0 = \sqrt{m_q^{*2} + \mathbf{p}_q^2} + \sqrt{m_{\bar{q}}^{*2} + \mathbf{p}_{\bar{q}}^2}. \quad (18)$$

The effective potential $V_{q\bar{q}}$ between the quark and antiquark in the rest frame of meson is comprised of linear confining potential V_{Conf} , the one-gluon-exchange Coulomb potential V_{Coul} , and the hyperfine potential V_{Hyp} (essential to distinguish between the pseudoscalar (0^{-+}) and vector (1^{--}) mesons) and is defined as

$$V_{q\bar{q}} = \underbrace{a + br}_{\text{conf}} - \underbrace{\frac{4\alpha_s}{3r}}_{\text{coul}} + \underbrace{\frac{32\pi\alpha_s \langle \mathbf{S}_q \cdot \mathbf{S}_{\bar{q}} \rangle}{9m_q^* m_{\bar{q}}^*}}_{\text{hyp}} \delta^{(3)}(r), \quad (19)$$

here a and b parameterize the linear confining potential, α_s is the strong running coupling, and the spin term $\langle \mathbf{S}_q \cdot \mathbf{S}_{\bar{q}} \rangle$ yields the values of $1/4$ and $-3/4$ for the vector and pseudoscalar mesons, respectively.

The LFWF is characterized by Lorentz-invariant internal variables, such as the longitudinal momentum fraction $x_j = \frac{p_j^+}{P^+}$, intrinsic transverse momentum $\mathbf{k}_{\perp j} = \mathbf{p}_{\perp j} - x_j \mathbf{P}_{\perp}$, along with the pair (p_j, λ_j) which denotes the on-mass-shell light-front momentum and the helicity of the quark

or antiquark ($j = q/\bar{q}$), respectively. In the momentum space, the LFWF is given by [48, 66]

$$\Psi_{\lambda_q \lambda_{\bar{q}}}^{JJ_z}(x, \mathbf{k}_\perp) = \Phi(x, \mathbf{k}_\perp) \mathcal{R}_{\lambda_q \lambda_{\bar{q}}}^{JJ_z}(x, \mathbf{k}_\perp), \quad (20)$$

where $\Phi(x, \mathbf{k}_\perp)$ and $\mathcal{R}_{\lambda_q \lambda_{\bar{q}}}^{JJ_z}(x, \mathbf{k}_\perp)$ denote the vacuum radial wave function and interaction independent spin-orbit wave function, respectively, the latter distinguishing between vector D^* and pseudoscalar D mesons. As discussed before, the in-medium effects on the properties of D mesons are simulated through the effective quark masses. The radial wave function $\Phi(x, \mathbf{k}_\perp)$ and the spin-orbit wave function $\mathcal{R}_{\lambda_q \lambda_{\bar{q}}}^{JJ_z}(x, \mathbf{k}_\perp)$ depend upon the quark masses and hence, will be modified at finite density of the medium, compared to free space. The explicit form of $\mathcal{R}_{\lambda_q \lambda_{\bar{q}}}^{*JJ_z}(x, \mathbf{k}_\perp)$ is expressed as (arising from the Melosh transformation) [48]

$$\mathcal{R}_{\lambda_q \lambda_{\bar{q}}}^{*00} = \frac{1}{\sqrt{2} \sqrt{\mathcal{A}^{*2} + \mathbf{k}_\perp^2}} \begin{pmatrix} -k^L & \mathcal{A}^* \\ -\mathcal{A}^* & -k^R \end{pmatrix} \quad (21)$$

and

$$\mathcal{R}_{\lambda_q \lambda_{\bar{q}}}^{*11} = \frac{1}{\sqrt{\mathcal{A}^{*2} + \mathbf{k}_\perp^2}} \begin{pmatrix} \mathcal{A}^* + \frac{\mathbf{k}_\perp^2}{\mathcal{M}^*} & k^R \frac{\mathcal{M}_1^*}{\mathcal{M}^*} \\ -k^R \frac{\mathcal{M}_2^*}{\mathcal{M}^*} & -\frac{(k^R)^2}{\mathcal{M}^*} \end{pmatrix}, \quad (22)$$

$$\mathcal{R}_{\lambda_q \lambda_{\bar{q}}}^{*10} = \frac{1}{\sqrt{2} \sqrt{\mathcal{A}^{*2} + \mathbf{k}_\perp^2}} \begin{pmatrix} k^L \frac{\mathcal{M}_3^*}{\mathcal{M}^*} & \mathcal{A}^* + \frac{2\mathbf{k}_\perp^2}{\mathcal{M}^*} \\ \mathcal{A}^* + \frac{2\mathbf{k}_\perp^2}{\mathcal{M}^*} & -k^R \frac{\mathcal{M}_3^*}{\mathcal{M}^*} \end{pmatrix}, \quad (23)$$

$$\mathcal{R}_{\lambda_q \lambda_{\bar{q}}}^{*1-1} = \frac{1}{\sqrt{\mathcal{A}^{*2} + \mathbf{k}_\perp^2}} \begin{pmatrix} -\frac{(k^L)^2}{\mathcal{M}^*} & k^L \frac{\mathcal{M}_2^*}{\mathcal{M}^*} \\ -k^L \frac{\mathcal{M}_1^*}{\mathcal{M}^*} & \mathcal{A}^* + \frac{\mathbf{k}_\perp^2}{\mathcal{M}^*} \end{pmatrix}, \quad (24)$$

for pseudoscalar and vector mesons, respectively. Here, $k^{R(L)} = k_x + ik_y$, $\mathcal{A}^* = (1-x)m_q^* + xm_{\bar{q}}^*$, $\mathcal{M}^* = M_0^* + m_q^* + m_{\bar{q}}^*$, $\mathcal{M}_1^* = xM_0^* + m_q^*$, $\mathcal{M}_2^* = (1-x)M_0^* + m_{\bar{q}}^*$ and $\mathcal{M}_3^* = \mathcal{M}_2^* - \mathcal{M}_1^*$. Asterik (*) sign symbolize that the quantities are medium dependent. The boost invariant mass of meson squared, M_0^{*2} is defined as

$$M_0^{*2} = \frac{\mathbf{k}_\perp^2 + m_q^{*2}}{x} + \frac{\mathbf{k}_\perp^2 + m_{\bar{q}}^{*2}}{1-x}. \quad (25)$$

Additionally, the spin-orbit wave functions $\mathcal{R}_{\lambda_q \lambda_{\bar{q}}}^{JJ_z}$ automatically satisfy the unitary condition $\langle \mathcal{R}_{\lambda_q \lambda_{\bar{q}}}^{JJ_z} | \mathcal{R}_{\lambda_q \lambda_{\bar{q}}}^{JJ_z} \rangle = 1$. To use a variational principle, we employ the lowest-order harmonic oscillator wave function as the in-medium trial radial wave function $\Phi^*(x, \mathbf{k}_\perp)$ for both pseudoscalar and vector mesons,

$$\Phi_{1S}^*(x, \mathbf{k}_\perp) = \frac{4\pi^{3/4}}{\beta^{3/2}} \sqrt{\frac{\partial k_z^*}{\partial x}} e^{-\frac{\mathbf{k}^2}{2\beta^2}}. \quad (26)$$

where β is the variational parameter controlling the wavefunction scale in our mass spectroscopic analysis, and is determined by applying the variational principle, under the condition that α_s is uniform across all the mesons. The variable transformation $\{k_z, \mathbf{k}_\perp\} \rightarrow \{x, \mathbf{k}_\perp\}$ involves the Jacobian,

$$\frac{\partial k_z^*}{\partial x} = \frac{M_0^*}{4x(1-x)} \left[1 - \frac{(m_q^{*2} - m_{\bar{q}}^{*2})^2}{M_0^{*4}} \right], \quad (27)$$

where longitudinal component $k_z^* = (x - 1/2) M_0^* + (m_{\bar{q}}^{*2} - m_q^{*2})/2M_0^*$. It is important to mention that the normalized LFWF will be utilized for additional computations [49].

We perform the variational analysis to evaluate the expectation value of the QCD motivated Hamiltonian $H_{q\bar{q}}$ with the trial function $\Phi_{1S}^*(x, \mathbf{k}_\perp)$ which has variational parameter β dependence. Once the parameter fixing is done by minimizing the expectation value, we can determine the mass eigenvalue of the meson as $M_{q\bar{q}}^* = \langle \Psi_{q\bar{q}} | H_{q\bar{q}} | \Psi_{q\bar{q}} \rangle = \langle \Phi_{1S}^* | H_{q\bar{q}} | \Phi_{1S}^* \rangle$. In order to avoid negative infinity, a Gaussian smearing function is used to weaken the singularity such that $\delta^3(\mathbf{r}) \rightarrow (\kappa^3/\pi^{3/2})e^{-\kappa^2 \mathbf{r}^2}$ [67]. Finally, the in-medium masses of D and D^* mesons are evaluated using the expression [49, 64]

$$M_{q\bar{q}}^* = \frac{\beta}{\sqrt{\pi}} \sum_{i=q, \bar{q}} z_i e^{z_i/2} \mathbf{K}_1\left(\frac{z_i}{2}\right) + a + \frac{2b}{\beta \sqrt{\pi}} - \frac{8\alpha_s \beta}{3 \sqrt{\pi}} + \frac{32\alpha_s \beta^3 \langle \mathbf{S}_q \cdot \mathbf{S}_{\bar{q}} \rangle}{9 \sqrt{\pi} m_q^* m_{\bar{q}}^*}. \quad (28)$$

where $z_i = m_i^{*2}/\beta^2$ and \mathbf{K}_1 is the modified Bessel function of the second kind.

III. RESULTS AND DISCUSSION

In this section, we present our results for the medium-modified masses, weak decay constants, and DAs for the pseudoscalar mesons D^0, D^+, D_s and vector mesons D^{0*}, D^{+*}, D_s^* . We analyze the

influence of finite baryon density ρ_B , isospin asymmetry η , and temperature T on the in-medium properties of mesons by incorporating effective quark masses derived using the CQMF model. The parameters utilized to solve the equations of motion to derive the density and temperature dependence of the scalar fields (σ, ζ, δ) and vector fields (ω, ρ) are detailed in Table I. The vacuum value of χ_0 and the coupling constant g_4 are fitted to the effective nucleon mass. The parameter ξ is determined from the QCD β -function at one loop level for three colors and three flavours [54]. The value of parameters k_0, k_1, k_2, k_3 and k_4 used in Eq. (8), are determined utilizing the π meson mass, m_π , K meson mass, m_K and the averaged mass of η and η' mesons [59]. The vacuum expectation values of the scalar meson fields σ and ζ represented by σ_0 and ζ_0 , are defined using the decay constants of the pion (f_π) and the kaon (f_K). These are given by the relations $\sigma_0 = -f_\pi$ and $\zeta_0 = \frac{1}{2}(f_\pi - 2f_K)$ [59]. The values of constituent quark masses in the free space (in units of GeV) and other potential parameters obtained by fitting the ground state mass spectra of D^0 and D^{0*} mesons are summarized as $m_{u/d} = 0.256$ GeV, $m_s = 0.457$ GeV, $m_c = 1.27$ GeV [68], $\alpha_s = 0.565$ GeV, $a = -0.043$ GeV, $b = 0.18$ GeV² [49] and $\kappa = 0.451$ [69]. The β parameters for the pseudoscalar D and vector D^* mesons computed by the variational principle (in the units of GeV) are given in Table II.

The masses of the ground state pseudoscalar D^0, D^+, D_s and vector D^{0*}, D^{+*}, D_s^* mesons calculated using the above discussed model parameters are given in Table III. We compared our findings with experimental data [68] and previously obtained results via LFQM [67] and QCD sum rules [70]. Our predicted meson masses are in good agreement with those obtained from LFQM and QCD sum rules, and are consistent with experimental data [68]. The calculated weak decay constants in vacuum are presented in Table IV, alongside results from lattice QCD [71], QCD sum rules [70], the Bethe-Salpeter (BS) model [72, 73], in addition to the experimental data [68]. For pseudoscalar D mesons, our predictions are in reasonable agreement with those from the BS model, whereas for the case of vector D^* mesons, our results show closer agreement with lattice QCD and QCD sum rules.

A. In-medium masses of D and D^* meson

Using the effective quark masses m_q^* obtained from the CQMF model in Eq. (28), the in-medium masses of pseudoscalar D and vector D^* mesons are calculated in an isospin asymmetric nuclear medium. The variation of the medium-modified masses of pseudoscalar D^0, D^+ and D_s mesons

| | | | | |
|---------------------------|--------------------------------------|----------------|---------------------|--------------------------|
| k_0 | k_1 | k_2 | k_3 | k_4 |
| 4.94 | 2.12 | -10.16 | -5.38 | -0.06 |
| σ_0 (MeV) | ζ_0 (MeV) | χ_0 (MeV) | ξ | $\rho_0(\text{fm}^{-3})$ |
| -92.8 | -96.5 | 254.6 | 6/33 | 0.16 |
| $g_\sigma^u = g_\sigma^d$ | $g_\sigma^s = g_\zeta^u = g_\zeta^d$ | g_δ^u | $g_\zeta^s = g_s$ | g_4 |
| 2.72 | 0 | 2.72 | 3.847 | 37.4 |
| $g_\delta^p = g_\delta^u$ | $g_\omega^N = 3g_\omega^u$ | g_ρ^p | $m_\pi(\text{MeV})$ | $m_K(\text{MeV})$ |
| 2.72 | 9.69 | 8.886 | 139 | 494 |
| $f_\pi(\text{MeV})$ | $f_K(\text{MeV})$ | g_δ^s | | |
| 92.8 | 115 | 0 | | |

TABLE I: List of model parameters used in the present work [52, 59].

| | | | |
|----------|--------------------|--------------------|--------------------|
| J^{PC} | $\beta_{c\bar{u}}$ | $\beta_{c\bar{d}}$ | $\beta_{c\bar{s}}$ |
| 0^{-+} | 0.5331 | 0.5189 | 0.6066 |
| 1^{--} | 0.4896 | 0.4681 | 0.4742 |

TABLE II: Gaussian parameter β for pseudoscalar mesons (D^0 , D^+ , D_s) and vector mesons (D^{0*} , D^{+*} , D_s^*), determined using the variational principle.

as a function of baryon density ρ_B (in units of nuclear saturation density ρ_0) for different values of temperatures $T = 0, 0.1$, and 0.15 GeV is shown in Fig. 1. In each subplot, the results are plotted for the isospin asymmetry values $\eta = 0, 0.3$, and 0.5 . For all three pseudoscalar mesons, the effective mass decreases with increasing ρ_B . The reduction is more pronounced for D^0 and D^+ mesons compared to the D_s meson. This is due to the presence of lighter u and d quarks in the former, which are more sensitive to medium effects. As shown in Figs. 1(a) and 1(d), isospin asymmetry significantly impacts the behavior of the members of isospin doublet $D = \begin{pmatrix} D^+ \\ D^0 \end{pmatrix}$ in the nuclear matter. The mass of D^0 meson increases notably as η rises from 0 to 0.5. For the D^+ meson, the in-medium mass increases slightly as η changes from 0 to 0.3. However, at low baryon densities,

| | Mass of Meson (GeV) | | | | | |
|--------------------|---------------------|-----------|-----------------|-----------------|--------------|-----------------|
| | M_{D^0} | M_{D^+} | M_{D_s} | $M_{D^{0*}}$ | $M_{D^{+*}}$ | $M_{D_s^*}$ |
| Present Work | 1.865 | 1.868 | 2.010 | 2.007 | 2.009 | 2.112 |
| Exp.[68] | 1.865 | 1.869 | 1.968 | 2.007 | 2.010 | 2.112 |
| LFQM [67] | 1.875 | - | 1.981 | 1.962 | - | 2.031 |
| QCD sum rules [70] | 1.87 ± 0.10 | - | 1.97 ± 0.10 | 2.01 ± 0.08 | - | 2.11 ± 0.07 |

TABLE III: Predicted ground-state mass spectra (in GeV) of pseudoscalar (D^0 , D^+ , D_s) and vector (D^{0*} , D^{+*} , D_s^*) mesons, compared with experimental data from Ref. [68] and other theoretical model predictions.

| | Weak Decay Constant (MeV) | | | | | |
|--------------------|---------------------------|--------------|------------------------|------------------------|--------------|-------------------------|
| | f_{D^0} | f_{D^+} | f_{D_s} | $f_{D^{0*}}$ | $f_{D^{+*}}$ | $f_{D_s^*}$ |
| Present Work | 234 | 228 | 285 | 282 | 268 | 280 |
| Exp.[68] | 206 | - | 257 | 239 | - | - |
| Lattice QCD [71] | $211 \pm 14_{-12}^{+0}$ | - | $231 \pm 12_{-1}^{+6}$ | $245 \pm 20_{-2}^{+0}$ | - | $272 \pm 16_{-20}^{+0}$ |
| QCD sum rules [70] | 208 ± 10 | - | 240 ± 10 | 263 ± 21 | - | 308 ± 21 |
| BS [72, 73] | 230 ± 25 | 230 ± 25 | 248 ± 27 | 340 ± 23 | 340 ± 23 | 375 ± 24 |

TABLE IV: Predicted weak decay constants (in MeV) for pseudoscalar (D^0 , D^+ , D_s) and vector (D^{0*} , D^{+*} , D_s^*) mesons in the free space, compared with experimental data from Ref. [68] and other theoretical model predictions.

effective mass of D^+ mesons is observed to be less at $\eta = 0.5$ compared to 0.3. This splitting in the effective masses of D^0 and D^+ mesons originates from the scalar-isoscalar field δ , which becomes non-zero in an isospin asymmetric medium. Because $I^{3u} = 1/2 = -I^{3d}$, the resulting difference between the effective masses of u and d quarks leads to a difference in the in-medium masses of D^0 and D^+ mesons. Additionally, as the temperature increases, the mass difference attributed to isospin asymmetry for the D^0 meson becomes less pronounced, as shown in Figs. 1(b) and 1(c). In contrast, for the D^+ meson, increasing the temperature from $T = 0$ to 0.15 GeV, gradually reverses the trend, with its effective mass decreasing under higher isospin asymmetry,

as illustrated in Fig. 1(f). For a symmetric nuclear medium ($\eta = 0$) at $\rho_B = \rho_0(3\rho_0)$, the mass shifts of D^0 meson are found to be $-0.097(-0.354)$, $-0.078(-0.275)$, and $-0.067(-0.234)$ GeV at temperatures $T = 0, 0.1$, and 0.15 GeV, respectively. When isospin asymmetry is introduced with $\eta = 0.5$, the corresponding shifts reduce to $-0.085(-0.227)$, $-0.07(-0.199)$, and $-0.066(-0.194)$ GeV from its vacuum mass of 1.865 GeV. For the D^+ meson, at $\eta = 0$, the mass shifts are observed to be $-0.095(-0.345)$, $-0.077(-0.268)$, and $-0.067(-0.229)$ GeV at the same temperatures and densities. Under isospin asymmetry $\eta = 0.5$, values of mass shifts change to $-0.103(-0.342)$, $-0.085(-0.289)$, and $-0.078(-0.269)$ GeV, indicating that the effective mass of the D^+ meson decreases with higher isospin asymmetry (except for higher baryon densities at $T = 0$ GeV).

The in-medium masses of the vector mesons D^{0*} , D^{+*} , and D_s^* are illustrated in Fig. 2 as a function of baryon density ρ_B (in units of ρ_0) for temperatures $T = 0, 0.1$, and 0.15 GeV. Each subplot presents results for isospin asymmetry values $\eta = 0, 0.3$, and 0.5 . At fixed isospin asymmetry and temperature of the medium, the effective masses of the D^{0*} and D^{+*} mesons are observed to decrease at lower densities and subsequently increase at higher ρ_B , whereas the D_s^* meson displays a gradual mass decrease with increasing density. This contrasting behaviour between pseudoscalar D and vector D^* mesons can be explained by the spin-spin interaction term in Eq. (19), where the expectation value $\langle \mathbf{S}_q \cdot \mathbf{S}_{\bar{q}} \rangle$ takes a value of $+1/4$ for vector mesons and $-3/4$ for pseudoscalar mesons. Consequently, the hyperfine potential V_{Hyp} acts to reduce the mass of pseudoscalar D mesons while increasing that of vector D^* mesons with increasing density. This effect is explicitly illustrated in Fig. 3, which shows the density dependence of effective masses of D and D^* mesons at $T = 0$ GeV and $\eta = 0$. Specifically, Figs. 3(a) and 3(c), clearly demonstrate that D^0 mass decreases, while D^{0*} mass increases in the presence of V_{Hyp} term at large baryon densities. Isospin asymmetry is observed to cause splitting in the effective masses of isospin doublet $D^* = \begin{pmatrix} D^{+*} \\ D^{0*} \end{pmatrix}$, due to the mass difference between u and d quarks in an isospin asymmetric nuclear medium. As shown in Figs. 2(a)-2(c), the effective mass of the D^{0*} meson remains largely unaffected by isospin asymmetry for low baryon densities, specifically, up to $\rho_B \sim \rho_0$ at $T = 0$ GeV, $\sim 1.5\rho_0$ at $T = 0.1$ GeV, and $\sim 2\rho_0$ at $T = 0.15$ GeV. At higher densities, a reduction in the effective masses due to isospin asymmetry is observed, although the overall magnitude of the mass splitting diminishes with rising temperature. At $\rho_B = 3\rho_0$, the observed mass shifts of D^{0*} , for $\eta = 0(0.5)$, are $0.028(-0.003)$, $0.008(-0.008)$, and $0.001(-0.007)$ GeV at $T = 0, 0.1$, and 0.15 GeV, respectively, relative to its vacuum mass of 2.007 GeV. For the D^{+*} meson, the response of the isospin

asymmetry differs. In Figs. 2(d), (e), and (f), the mass of D^{+*} is observed to rise as η goes from 0 to 0.3. However, for $\eta = 0.5$, the effective mass decreases in Fig. 2(d) and gradually shows an increase in Fig. 2(f). At $\rho_B = 3\rho_0$ and $\eta = 0(0.5)$, the mass shifts for D^{+*} meson are observed to be 0.02(0.019), 0.02(0.007) and 0.02(0.005) GeV from its vacuum value corresponding to $T = 0, 0.1$ and 0.15 GeV, respectively.

Expanding the analysis to include the pseudoscalar D_s and vector D_s^* mesons shows that both mesons demonstrate qualitatively similar behaviour as the baryon density rises, though with differing magnitudes. As shown in Figs. 3(b) and 3(d), for given baryon density, the effective mass of the D_s meson decreases while that of D_s^* meson increases when the hyperfine interaction term V_{Hyp} is included in the calculations. This is attributed to the reduced influence of nuclear medium and the greater mass of s quark relative to the u/d quarks, leading to smaller fluctuations in the V_{Hyp} term as baryon density rises. An increase in the isospin asymmetry of the medium causes a rise in the effective masses of D_s and D_s^* mesons which is more pronounced at lower temperatures. As shown in subplots (g) and (i) of Figs. 1 and 2, the effective mass increases slightly with η , but this trend becomes less distinct as temperature rises. Nonetheless, at $T = 0.15$ GeV and $\rho_B < 3\rho_0$, the effective masses are found to overlap for $\eta = 0$ and 0.3, while it shows a decrease for $\eta = 0.5$. Beyond this density, there is a slight increase in the masses for $\eta = 0.3$ and 0.5. For $\eta = 0.5$, the mass shift of the D_s meson from its vacuum value of 2.008 GeV is $-0.029(-0.048)$ GeV, $-0.026(-0.045)$, and $-0.023(-0.043)$ GeV at $T = 0, 0.1$, and 0.15 GeV, respectively at $\rho_B = \rho_0(3\rho_0)$. Similarly, the mass shift for the D_s^* meson from its vacuum value of 2.111 GeV is $-0.024(-0.039)$, $-0.021(-0.037)$, and $-0.02(-0.035)$ GeV at the same temperatures. These results indicate that the s quark experiences minimal modification in an isospin asymmetric medium. Meanwhile, an increase in medium temperature leads to a decrease in mass shift for all pseudoscalar D mesons and vector D^* mesons. Additionally, at $T = 0.15$ GeV isospin doublet mesons reveal a contrasting behavior with isospin asymmetry.

Several theoretical studies have reported significant modifications in the masses of pseudoscalar D and vector D^* mesons when placed in a nuclear medium. Using a chiral hadronic model, the mass of the D^0 meson in an isospin asymmetric nuclear medium was found to shift by -0.058 GeV, while the D^+ meson exhibited a larger shift of -0.099 GeV when η is set to 0.5 at nuclear saturation density [37]. Under similar conditions employing a combined chiral SU(3) and QCD sum-rule framework, mass shifts of -0.040 , -0.081 , -0.068 and -0.047 GeV were reported for D_s , D^{0*} , D^{+*} and D_s^* mesons, respectively, in an isospin asymmetric strange hadronic medium

[44, 47]. In symmetric nuclear medium, the quark-meson coupling model predicted a mass shift of -0.062 GeV for both D and \bar{D} mesons at a density of $\rho_B = 0.15 \text{ fm}^{-3}$ [36]. A mass splitting of 0.060 GeV for the $D - \bar{D}$ doublet at $\rho_B = 0.15 \text{ fm}^{-3}$ was found using QCD sum rules in cold nuclear medium [74]. Additionally, only a mild change in the mass of the D meson, but a significant broadening of its width was observed using a self-consistent coupled channel method [31]. In Ref. [43] the effects of symmetric nuclear medium was analysed on the vector D^* meson, where mass shifts of -0.076 , -0.071 , -0.065 and -0.056 GeV were observed at $T = 0, 0.05, 0.1$ and 0.15 GeV, respectively, at $\rho_B = \rho_0$.

B. In-medium weak decay constant of D and D^* meson

The decay constant is defined through the matrix elements connecting the vacuum to a meson state with four-vector momenta P for pseudoscalar mesons and vector mesons through relations [49, 75],

$$\langle 0 | \bar{q} \gamma^\mu \gamma_5 q | P(P) \rangle = i f_P P^\mu, \quad (29)$$

and

$$\langle 0 | \bar{q} \gamma^\mu q | V(P, J_z) \rangle = f_V M_V \epsilon^\mu(J_z), \quad (30)$$

respectively. Here, f_P and f_V are the decay constants for pseudoscalar and vector mesons, respectively. Also, $\epsilon^\mu(J_z)$ and M_V denote the polarization vector and the mass of the vector meson. The explicit forms of the medium-modified decay constants of pseudoscalar and vector mesons are given by [49]

$$f_P^* = 2\sqrt{6} \int_0^1 dx \int \frac{d^2 \mathbf{k}_\perp}{2(2\pi)^3} \frac{\Phi^*(x, \mathbf{k}_\perp)}{\sqrt{\mathcal{A}^{*2} + \mathbf{k}_\perp^2}} \mathcal{A}^*, \quad (31)$$

$$f_V^* = 2\sqrt{6} \int_0^1 dx \int \frac{d^2 \mathbf{k}_\perp}{2(2\pi)^3} \frac{\Phi^*(x, \mathbf{k}_\perp)}{\sqrt{\mathcal{A}^{*2} + \mathbf{k}_\perp^2}} \left(\mathcal{A}^* + \frac{2\mathbf{k}_\perp^2}{\mathcal{M}^*} \right). \quad (32)$$

The ratio of the weak decay constant in an isospin asymmetric nuclear medium to that in free space, f_M^*/f_M , is shown in Figs. 4 and 5. The variation of f_M^*/f_M for pseudoscalar mesons D^0 , D^+ and D_s and vector mesons D^{0*} , D^{+*} and D_s^* is plotted as a function of the baryon density ρ_B

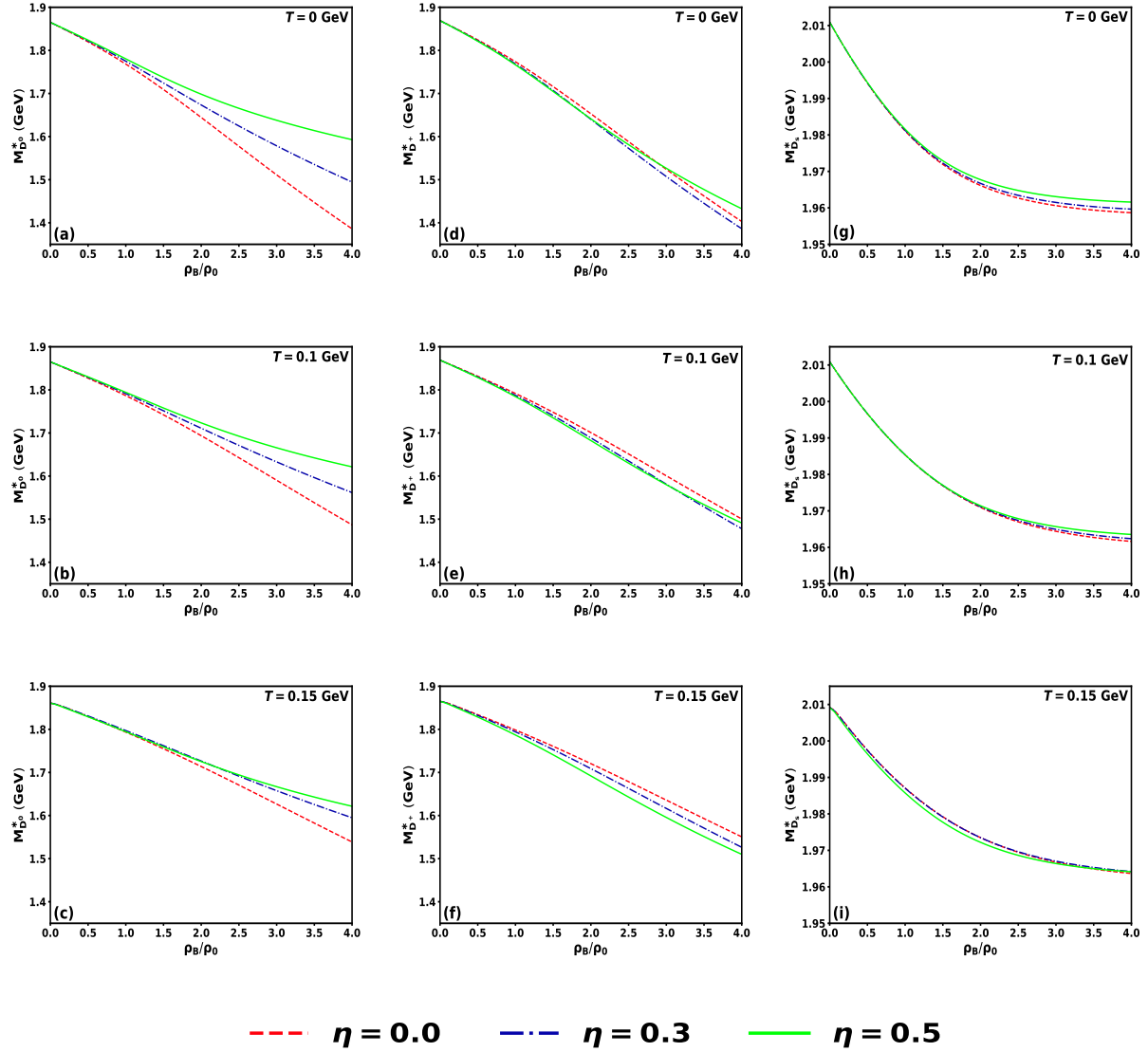


FIG. 1: In-medium masses of pseudoscalar D^0 , D^+ and D_s mesons as a function of baryon density ρ_B (in units of nuclear saturation density ρ_0). Results are shown for temperatures $T = 0$ GeV [subplots (a), (d) and (g)], $T = 0.1$ GeV [subplots (b), (e) and (h)] and $T = 0.15$ GeV [subplots (c), (f) and (i)] GeV, at isospin asymmetry values $\eta = 0, 0.3$ and 0.5 .

for different values of temperatures $T = 0, 0.1$ and 0.15 GeV. Each subplot presents results corresponding to the isospin asymmetry $\eta = 0, 0.3$ and 0.5 . The weak decay constant ratio is observed to decrease with increasing baryon density ρ_B for all pseudoscalar D and vector D^* mesons. Both pseudoscalar D and vector D^* mesons exhibit a similar trend in the weak decay constant ratio as the isospin asymmetry increases in the medium. However, the ratio for vector D^* mesons is higher in magnitude than that for pseudoscalar D mesons at any particular value of ρ_B . In an isospin sym-

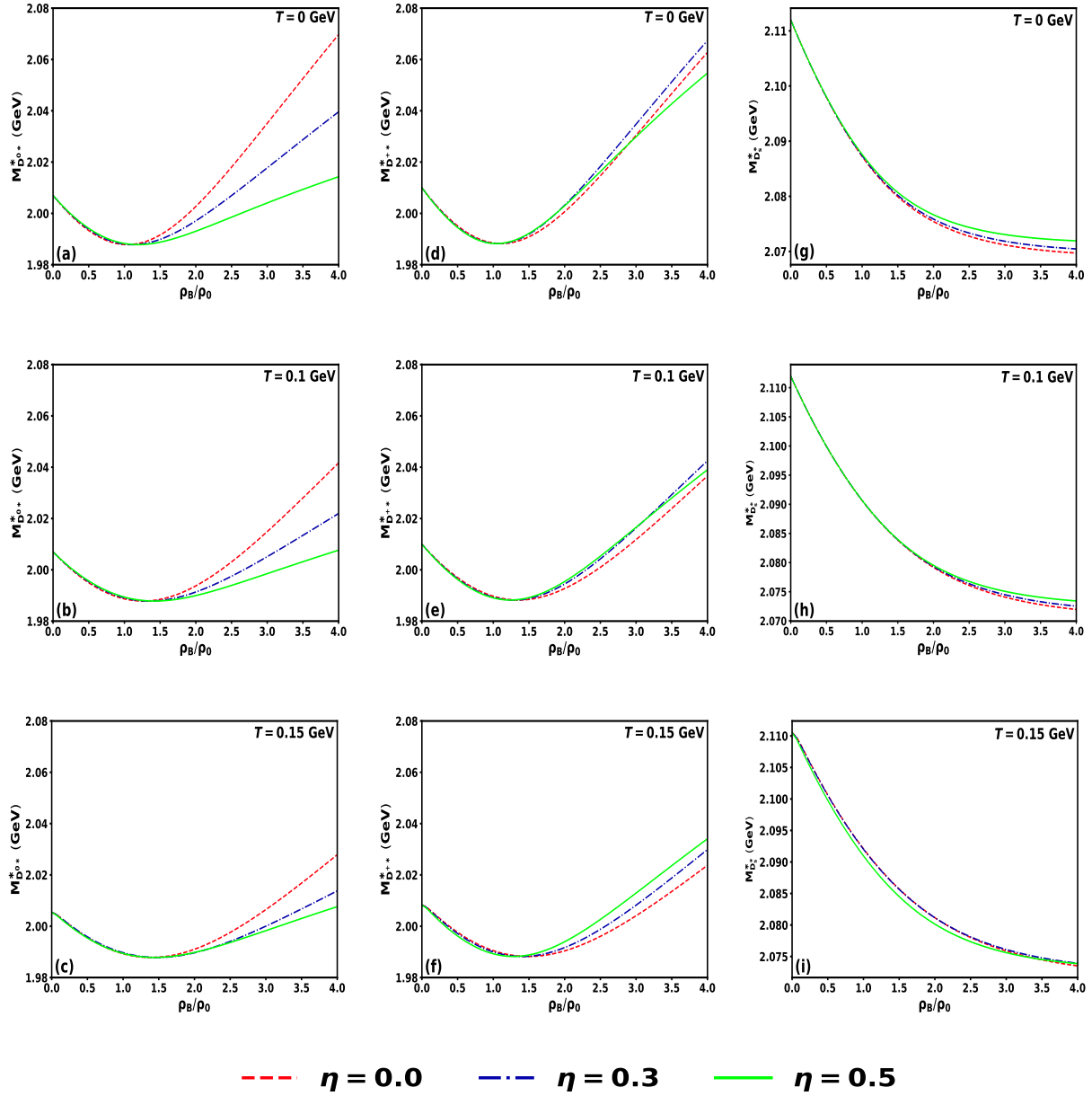


FIG. 2: In-medium masses of vector D^{0*} , D^{+*} and D_s^* mesons plotted as a function of baryon density ρ_B (in units of ρ_0). Results are shown for temperatures $T = 0$ GeV [subplots (a), (d) and (g)], $T = 0.1$ GeV [subplots (b), (e) and (h)] and $T = 0.15$ GeV [subplots (c), (f) and (i)] GeV, at isospin asymmetry values $\eta = 0, 0.3$ and 0.5 .

metric medium at $\rho_B = \rho_0(3\rho_0)$ and $T = 0$ GeV, the observed magnitude of the ratio is 0.936(0.855) for D^0 , 0.936(0.854) for D^+ , 0.986(0.975) for the D_s meson. In contrast, the corresponding values of the ratio for the vector D^{0*} , D^{+*} and D_s^* mesons are found to be 0.970(0.927), 0.970(0.925) and 0.997(0.994), respectively. This indicates that vector mesons experience reduced suppression

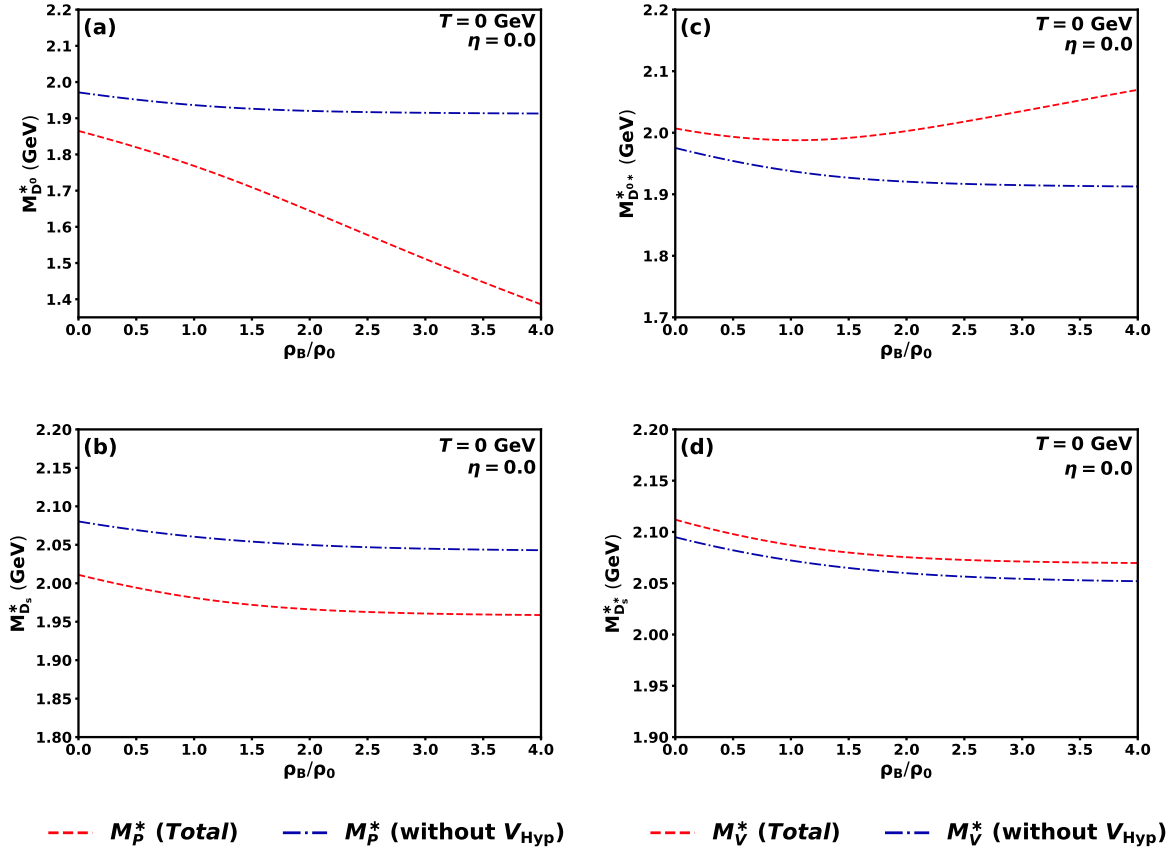


FIG. 3: In-medium masses of pseudoscalar D^0 and D_s mesons [left panel] and the vector D^{0*} and D_s^* mesons [right panel] as functions of baryon density ρ_B (in units of ρ_0) at temperature $T = 0$ GeV and isospin asymmetry $\eta = 0$. Results are shown both with and without the contribution of the hyperfine potential.

in the nuclear medium and can be understood through Eqs. (31) and (32). The additional term $2\mathbf{k}_\perp^2/M^*$ in Eq. (32) compensates for the reduction caused by the term \mathcal{A}^* , resulting in a higher value of weak decay constant for vector mesons.

As shown in Figs. 4(a)-4(c), the ratio for D^0 meson increases with increasing asymmetry, with a more pronounced rise at higher densities. The splitting in the ratios due to asymmetry decreases as the temperature increases from $T = 0$ to 0.15 GeV, and the influence of asymmetry emerges at higher ρ_B . For the D^+ meson, Fig. 4(d) shows a slight increase in the ratio at larger ρ_B when $\eta = 0.5$. However, when the temperature is raised to $T = 0.1$ GeV in Fig. 4(e), the ratio gradually decreases for the same η . In Fig. 4(f), a further increase in temperature yields a notable decline in the ratio as η increases. This contrasting behavior for the ratio of D^+ and D^0 mesons arises from the splitting of the constituent u and d quark masses in an isospin asymmetric medium. As shown

in Figs. 4(g) and (h), the ratio for the D_s meson increases as η increases at higher densities, while the effect of asymmetry diminishes for rising temperature. In Fig. 4(i), the ratio for D_s decreases at lower densities as η changes from 0 to 0.5, before rising at higher ρ_B . In contrast, the ratios for $\eta = 0$ and 0.3 remain identical. A similar pattern appears for the weak decay ratios of the vector mesons D^{0*} , D^{+*} , and D_s^* in Fig. 5. Each subplot mirrors that of the corresponding pseudoscalar mesons in Fig. 4, differing only in magnitude. Moreover, the pseudoscalar D_s and vector D_s^* meson exhibit minimal fluctuations across the parameter space, as indicated by the nearly constant values of $f_{D_s}^*/f_{D_s}$ and $f_{D_s^*}^*/f_{D_s^*}$ with the increasing η . This uniformity arises from the lower sensitivity of medium effects on the s quark. In contrast, the lighter u and d quarks undergo more substantial mass reduction in the nuclear medium, due to the partial restoration of chiral symmetry [59]. Table V illustrates these trends at $\rho_B = 3\rho_0$. To conclude, rising temperature generally enhances the decay constant ratios for both pseudoscalar and vector D mesons. Using a hybrid chiral SU(3) model combined with QCD sum rules, shifts in the weak decay constants have been studied in a strange hadronic medium [42, 44, 47]. Similarly, QCD sum rules were used in Ref. [76] to investigate decay constants of heavy mesons.

| Temperature T (GeV) | Isospin asymmetry η | Ratio of Decay Constants f_M^*/f_M | | | | | |
|--------------------------|--------------------------------|--------------------------------------|---------------------|---------------------|---------------------------|---------------------------|-------------------------|
| | | $f_{D^0}^*/f_{D^0}$ | $f_{D^+}^*/f_{D^+}$ | $f_{D_s}^*/f_{D_s}$ | $f_{D^{0*}}^*/f_{D^{0*}}$ | $f_{D^{+*}}^*/f_{D^{+*}}$ | $f_{D_s^*}^*/f_{D_s^*}$ |
| 0.00 | 0.0 | 0.855 | 0.854 | 0.975 | 0.927 | 0.925 | 0.994 |
| | 0.3 | 0.867 | 0.852 | 0.975 | 0.934 | 0.924 | 0.994 |
| | 0.5 | 0.882 | 0.855 | 0.976 | 0.942 | 0.926 | 0.995 |
| 0.10 | 0.0 | 0.870 | 0.870 | 0.977 | 0.936 | 0.934 | 0.995 |
| | 0.3 | 0.880 | 0.865 | 0.977 | 0.942 | 0.932 | 0.995 |
| | 0.5 | 0.890 | 0.865 | 0.977 | 0.947 | 0.932 | 0.995 |
| 0.15 | 0.0 | 0.878 | 0.878 | 0.978 | 0.94 | 0.939 | 0.995 |
| | 0.3 | 0.888 | 0.873 | 0.978 | 0.946 | 0.936 | 0.995 |
| | 0.5 | 0.890 | 0.868 | 0.978 | 0.947 | 0.933 | 0.995 |

TABLE V: Ratios of in-medium to vacuum weak decay constants f_M^*/f_M for pseudoscalar (D^0, D^+, D_s) and vector (D^{0*}, D^{+*}, D_s^*) mesons, at baryon density $\rho_B = 3\rho_0$ for different temperatures (T) and isospin asymmetry (η).

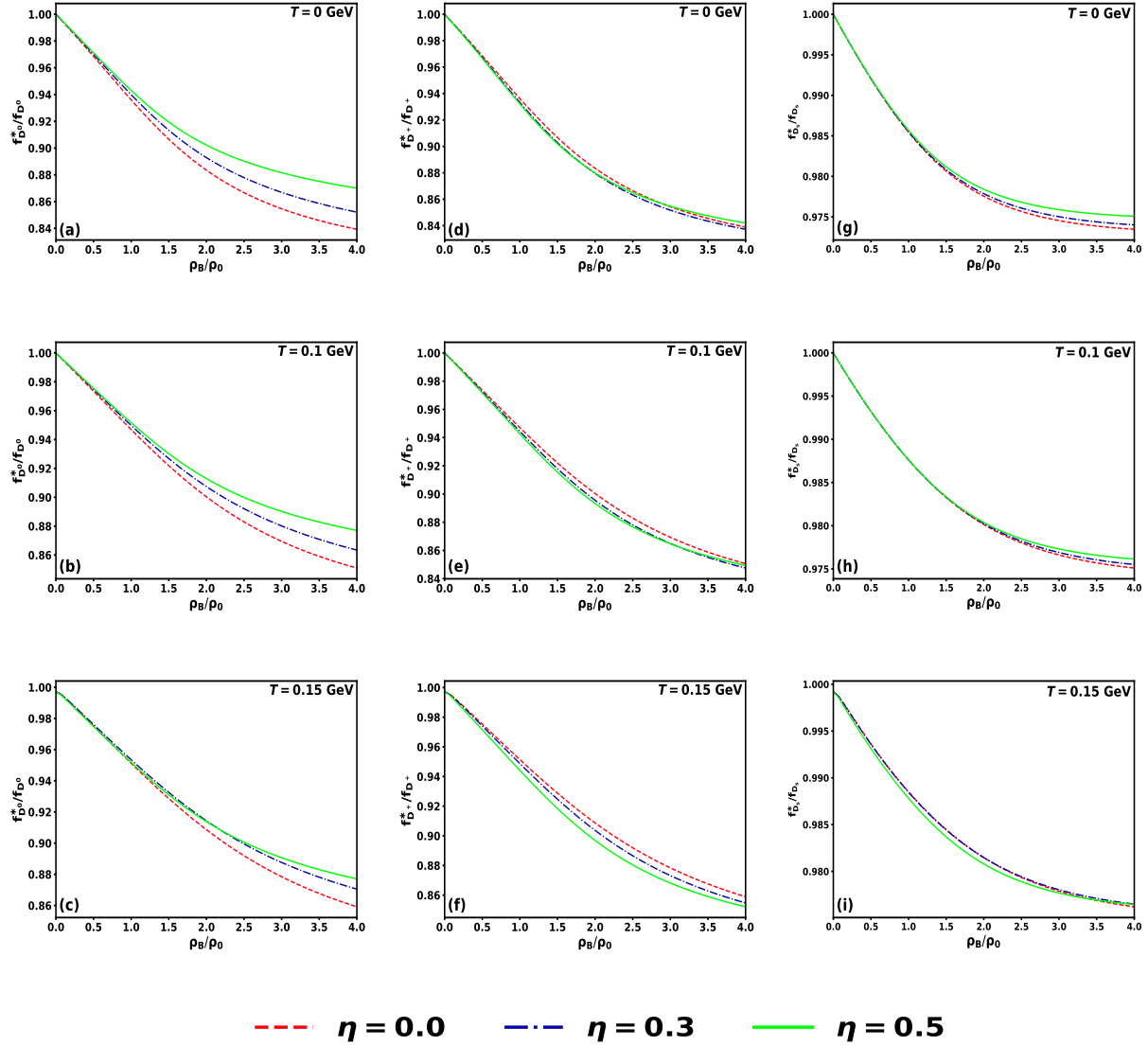


FIG. 4: The ratio of the in-medium weak decay constant to the free-space value for pseudoscalar D^0 , D^+ , and D_s mesons plotted as a function of baryon density (in units of ρ_0). The results are presented for temperature $T = 0$ [in subplots (a), (d) and (g)], 0.1 [in subplots (b), (e) and (h)] and 0.15 [in subplots (c), (f) and (i)] GeV at isospin asymmetry $\eta = 0, 0.3$ and 0.5 .

C. In-medium distribution amplitude

The leading twist quark DAs of the mesons describe the longitudinal momentum fraction carried by the valence-quarks and can be derived from hard exclusive reaction processes [77, 78]. These DAs are formally defined through matrix elements that connect free space states to meson states, and can be interpreted as the probability amplitudes for the hadron to be in its lowest Fock state with small separation in transverse momentum. The correlators for defining the pseudoscalar

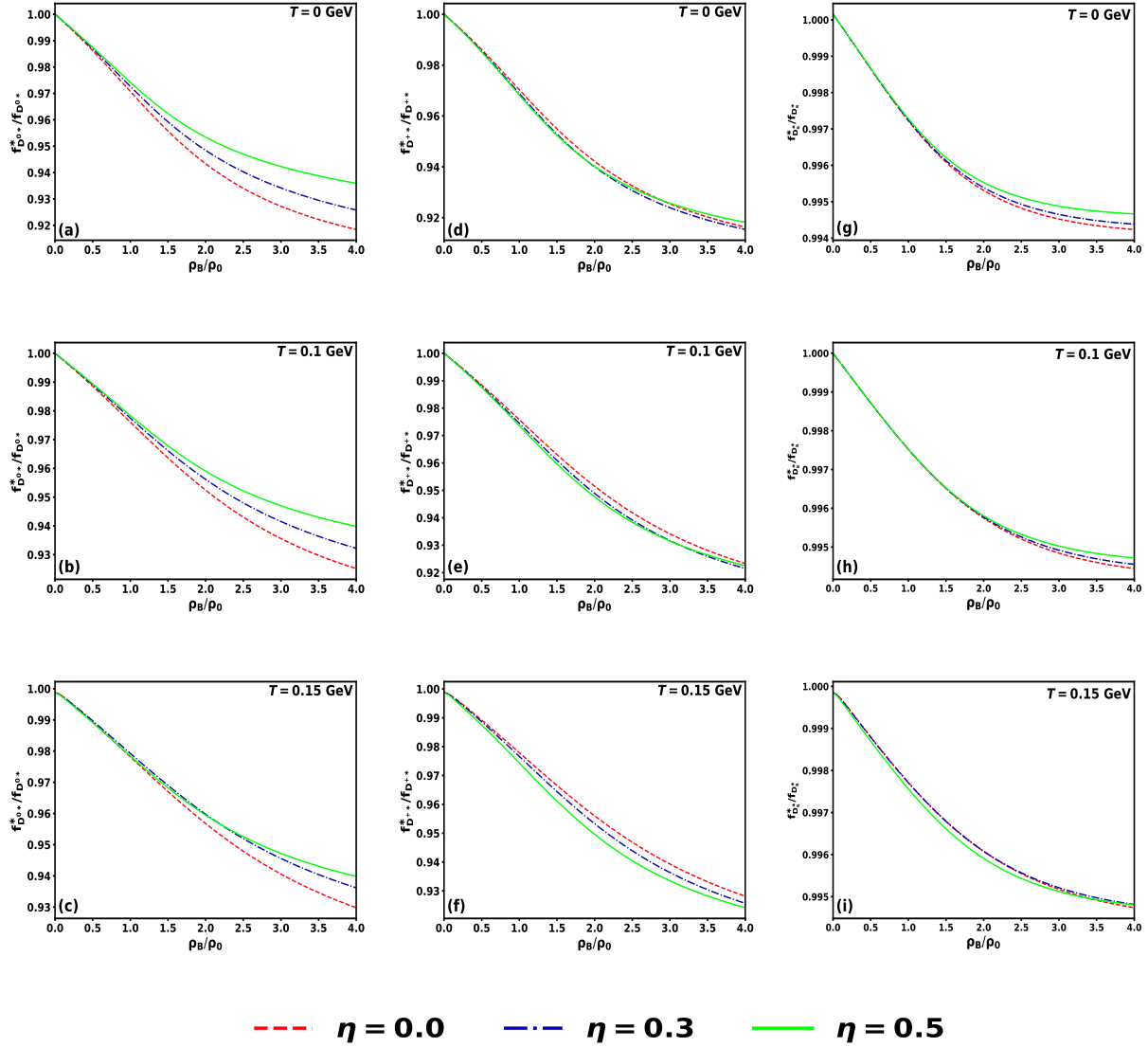


FIG. 5: The ratio of the in-medium weak decay constant to the free-space value for vector D^{0*} , D^{+*} and D_s^* mesons plotted as a function of baryon density (in units of ρ_0). The results are presented for temperature $T = 0$ [in subplots (a), (d), and (g)], 0.1 [in subplots (b), (e), and (h)], and 0.15 [in subplots (c), (f) and (i)] GeV at isospin asymmetry $\eta = 0, 0.3$ and 0.5 .

and vector mesons can be expressed as [49, 79, 80]

$$\begin{aligned}
 A_P^+ &= \langle 0 | \bar{q}(z) \gamma^+ \gamma_5 q(-z) | P(P) \rangle, \\
 &= i f_P P^+ \int_0^1 dx e^{i(2x-1)P \cdot z} \phi_P(x) \Big|_{z^+ = z_\perp = 0},
 \end{aligned} \tag{33}$$

$$\begin{aligned}
 A_V^+ &= \langle 0 | \bar{q}(z) \gamma^+ q(-z) | V(P, 0) \rangle, \\
 &= f_V M_V \epsilon^+(0) \int_0^1 dx e^{i(2x-1)P \cdot z} \phi_V(x) \Big|_{z^+ = z_\perp = 0}.
 \end{aligned} \tag{34}$$

The medium-modified $\phi_M^*(x)$ for pseudoscalar and vector mesons can be obtained by integrating the LFWF over transverse momentum as

$$\phi_P^*(x) = \frac{2\sqrt{6}}{f_P^*} \int \frac{d^2\mathbf{k}_\perp}{2(2\pi)^3} \frac{\Phi^*(x, \mathbf{k}_\perp)}{\sqrt{\mathcal{A}^{*2} + \mathbf{k}_\perp^2}} \mathcal{A}^*, \quad (35)$$

$$\phi_V^*(x) = \frac{2\sqrt{6}}{f_V^*} \int \frac{d^2\mathbf{k}_\perp}{2(2\pi)^3} \frac{\Phi^*(x, \mathbf{k}_\perp)}{\sqrt{\mathcal{A}^{*2} + \mathbf{k}_\perp^2}} \left(\mathcal{A}^* + \frac{2\mathbf{k}_\perp^2}{\mathcal{M}^*} \right). \quad (36)$$

There has been limited investigation in the literature on the determination of DAs for D mesons in a nuclear medium [49]. The behavior of the D meson DA in a vacuum has been studied using the revised light-cone harmonic oscillator model in Ref. [81]. Additionally, QCD sum rules have been employed within the background field theory framework to study the leading-twist light-cone DA of the D_s meson [82]. In this work, we present the DAs, $\phi_M^*(x)$, as a function of longitudinal momentum fraction x for both pseudoscalar D and vector D^* mesons for free space ($\rho_B = 0$) at temperature $T = 0$ GeV in Fig. 6. The DAs exhibit a convex-concave shape, indicating that the heavier charm quark carries the majority of the meson's momentum [83]. Moreover, our results are in qualitative agreement with those in Refs. [81, 82]. In addition, the DAs for pseudoscalar mesons having u or d quarks reach higher peaks than those with an s quark, due to the smaller mass difference between the strange and charm quarks. In contrast, the vector mesons exhibit an opposite trend, as the meson having s quark attains a higher peak. The difference arises from the additional term $2\mathbf{k}_\perp^2/\mathcal{M}^*$ in Eq. (36), which increases with baryon density, whereas the \mathcal{A}^* term decreases. The combined effect of these terms lead to overall higher DAs for the vector D^* mesons.

Fig. 7 presents the DAs for pseudoscalar D and vector D^* mesons as a function of longitudinal momentum fraction x , evaluated at baryon density $\rho_B = 3\rho_0$ and temperature $T = 0$ GeV, at $\eta = 0$ and 0.5. In the left panel, Fig. 7(a) indicates that the DAs for the D^0 and D^+ mesons are nearly identical in a symmetric medium. However, Fig. 7(b) shows that under isospin asymmetry ($\eta = 0.5$), a noticeable separation emerges between their DAs. The right panel displays the DAs for vector D^* mesons. In Fig. 7(c) corresponding to the symmetric case, the DAs for D^{0*} and D^{+*} are observed to overlap for $x < 0.24$, followed by a noticable distinction beyond this region. When isospin asymmetry is introduced as shown, in Fig. 7(d), the DA for the D^{0*} meson shifts slightly upward compared to that of the D^{+*} meson for $x < 0.24$. Beyond this point, both DAs remain nearly unchanged from those in Fig. 7(c). In contrast, the DAs for the pseudoscalar D_s and

vector D_s^* meson remain largely unaffected by isospin asymmetry. This stability is attributed to the presence of the s quark, which is less sensitive to medium effects. A similar behavior for the D and D^* mesons in symmetric nuclear medium was previously reported in Ref. [49].

The density variation of in-medium DAs of D and D^* mesons in an isospin asymmetric nuclear medium ($\eta = 0.5$) as a function of longitudinal momentum fraction x at temperature $T = 0$ GeV is represented in Fig. 8. As illustrated in Fig. 8(a), for $\rho_B = \rho_0$, the DAs of D^0 and D^+ mesons overlaps at lower x , but separate noticeably at higher values of x . However, for $\rho_B = 3\rho_0$, this separation becomes significant across the entire range of x . This behavior is attributed to the difference between the u and d quark masses induced by isospin asymmetry in the medium. The DA curves for D^0 and D^+ corresponding to higher density show a reduction in magnitude compared to the curves at $\rho_B = \rho_0$ for $x < 0.3$. In contrast, for larger values of x , there is a noticeable rise in magnitude, resulting in both curves converging around $x > 0.8$. The variation in DAs of vector D^* mesons is presented in Fig. 8(b). Here, DAs for D^{0*} and D^{+*} mesons also coincide at low x , while a clear splitting appears at higher x . However, the overall change in DAs for these mesons remains minor as the baryon density increases from $\rho_B = \rho_0$ to $3\rho_0$. A similar pattern in the behavior of DAs with baryon density for pseudoscalar and vector mesons is observed in Ref. [49]. For the pseudoscalar D_s and vector D_s^* mesons, the DAs remain largely unchanged near the endpoint $x \rightarrow 0$ and $x \rightarrow 1$ with increasing ρ_B . There is, however, a slight decrease in the DAs for $\rho_B = 3\rho_0$ within the interval $0.3 < x < 0.5$.

To investigate the influence of temperature on the DAs of pseudoscalar D and vector D^* mesons, we plot $\phi_M^*(x)$ as a function of longitudinal momentum fraction x , as shown in Fig. 9. The analysis is carried out for an isospin asymmetry $\eta = 0.5$ at two baryon densities $\rho_B = \rho_0$ and $3\rho_0$. Each subplot presents results at temperatures $T = 0$ and 0.1 GeV. For both densities, the DAs for the pseudoscalar D^0 , D^+ , and D_s mesons as well as the vector D^{0*} , D^{+*} and D_s^* mesons are noted to remain almost unchanged when temperatures increases from $T = 0$ to $T = 0.1$ GeV. However, a closer inspection of the peak values reveals small but noteworthy shifts with increasing baryon density. In particular, the maxima of the DA for the D^0 meson changes from 1.719(1.718) to 1.748(1.742), for the D^+ meson from 1.739(1.737) to 1.786(1.777), and for the D_s meson from 1.686(1.688) to 1.675(1.677) as ρ_B increases from ρ_0 to $3\rho_0$ at $T = 0(0.1)$ GeV. Similarly, for vector mesons, the peak of the DA for the D^{0*} meson shifts from 1.948(1.947) to 1.962(1.958), the D^{+*} meson from 1.888(1.89) to 1.908(1.903), and the D_s^* meson from 2.029(2.032) to 2.012(2.016), under the same conditions. These changes highlight the sensitivity of DAs to the baryon density,

even though their overall temperature dependence remains minimal in the range considered.

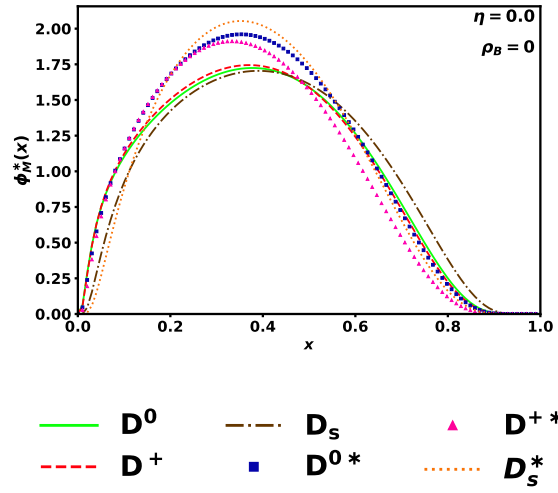


FIG. 6: Distribution amplitude $\phi_M^*(x)$ plotted as a function of longitudinal momentum fraction x for pseudoscalar (D^0 , D^+ and D_s) and vector (D^{0*} , D^{+*} and D_s^*) mesons in free space ($\rho_B = 0$) at temperature $T = 0$ GeV.

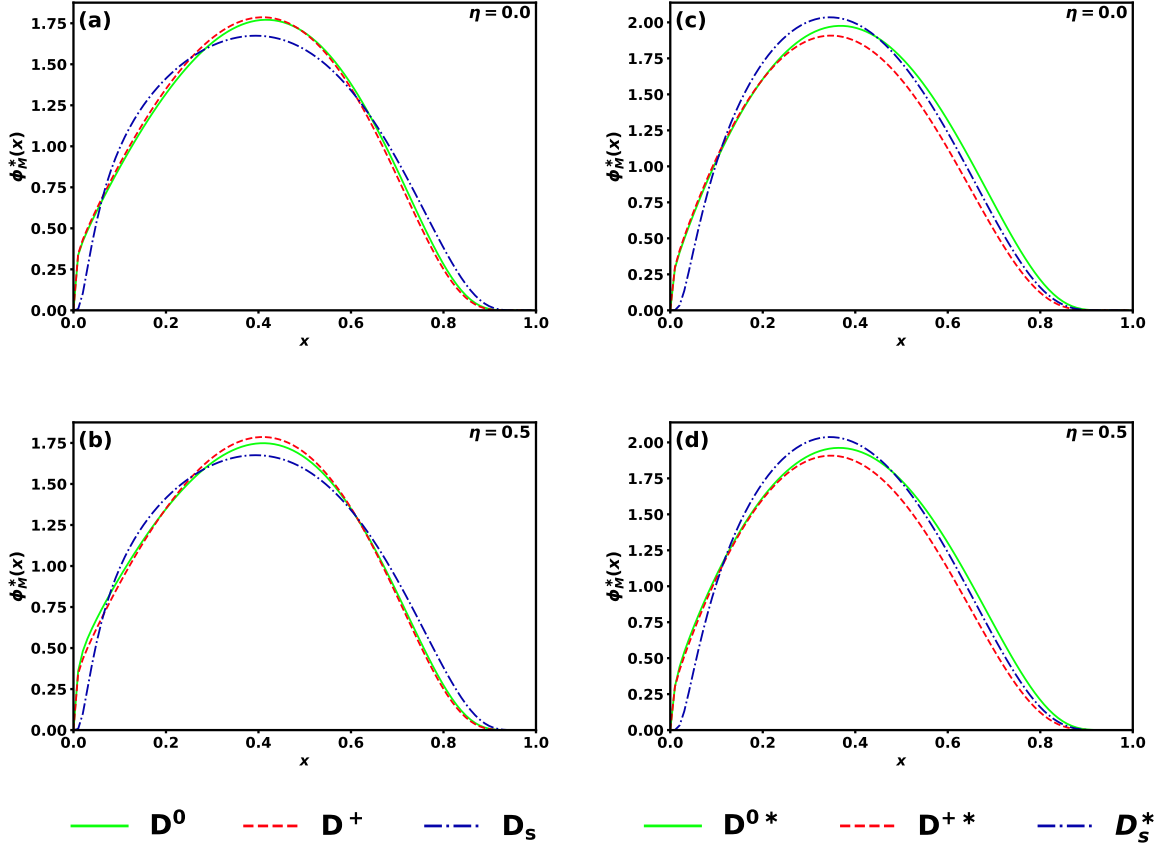


FIG. 7: Distribution amplitudes $\phi_M^*(x)$ for pseudoscalar (D^0 , D^+ and D_s) mesons [left panel] and vector (D^{0*} , D^{+*} and D_s^*) mesons [right panel] plotted as a function of longitudinal momentum fraction x at baryon density $\rho_B = 3\rho_0$ and temperature $T = 0$ GeV. The results are presented for symmetric nuclear medium ($\eta = 0.0$) [in subplots (a) and (c)] and isospin asymmetric nuclear medium ($\eta = 0.5$) [in subplots (b) and (d)].

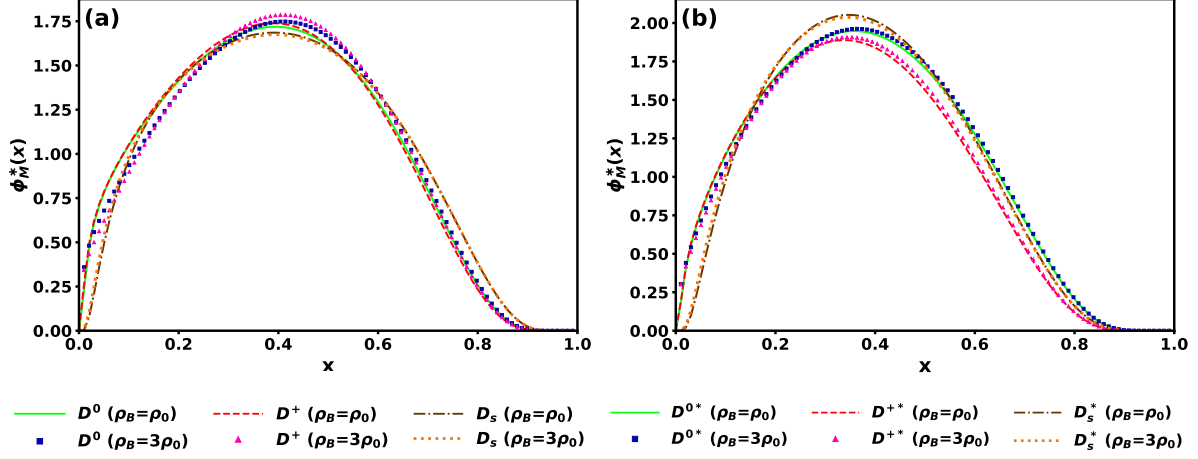


FIG. 8: Distribution amplitudes $\phi_M^*(x)$ plotted as a function of longitudinal momentum fraction x for pseudoscalar mesons (D^0 , D^+ and D_s) [left panel] and vector mesons (D^{0*} , D^{+*} and D_s^*) [right panel] at isospin asymmetry $\eta = 0.5$ and temperature $T = 0$ GeV. Each subplot displays results for baryon densities $\rho_B = \rho_0$ and $3\rho_0$.

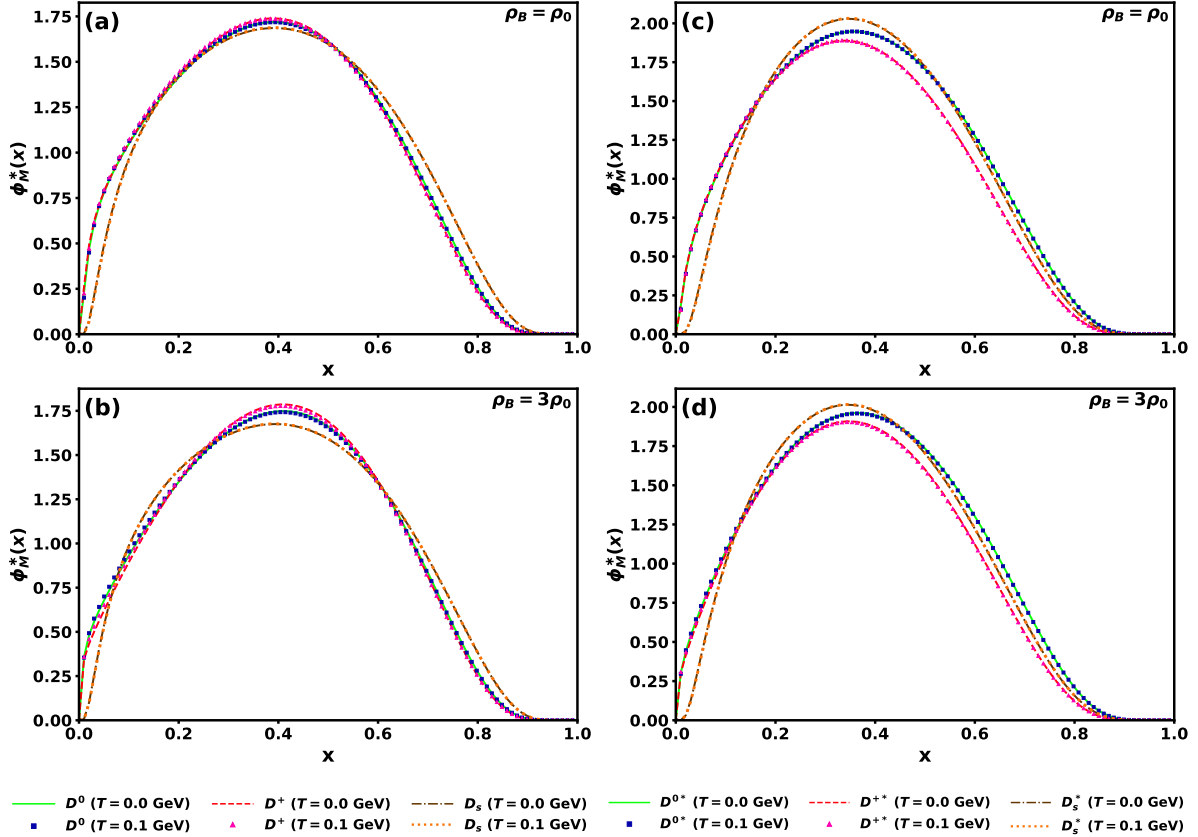


FIG. 9: Distribution amplitudes $\phi_M^*(x)$ for pseudoscalar mesons (D^0 , D^+ and D_s) [left panel] and vector mesons (D^{0*} , D^{+*} and D_s^*) [right panel] plotted as a function of longitudinal momentum fraction x at isospin asymmetry $\eta = 0.5$. The results are presented for baryon densities $\rho_B = \rho_0$ [in subplots (a) and (c)] and $3\rho_0$ [in subplots (b) and (d)] at temperature $T = 0$ and $T = 0.1$ GeV.

IV. SUMMARY

In this study, we investigated the medium modifications of pseudoscalar (D^0 , D^+ , D_s) and vector (D^{0*} , D^{+*} , D_s^*) mesons using a hybrid framework that combines the LFQM with the CQMF model. The in-medium quark masses, determined using the CQMF model were used as input in the LFQM to evaluate meson properties in an isospin asymmetric nuclear medium at zero and finite temperature.

We first determined the meson masses and weak decay constants in vacuum using the variational principle to calculate the Gaussian parameter β . These results were found to be comparable with the available experimental data and theoretical predictions. In-medium effects were analyzed over a range of baryon density (ρ_B) and isospin asymmetries (η). The masses of pseudoscalar D^0 and D^+ mesons were observed to decrease with increasing ρ_B , while that of vector D^* mesons, containing u or d quarks, initially decreased but increased at higher densities. The isospin asymmetry induced mass splitting within the isospin doublet $D = \begin{pmatrix} D^+ \\ D^0 \end{pmatrix}$ and $D^* = \begin{pmatrix} D^{+*} \\ D^{0*} \end{pmatrix}$. The pseudoscalar D_s and vector D_s^* mesons exhibited minimal sensitivity to isospin asymmetry due to the presence of the s quark. Furthermore, the effect of finite temperature was found to suppress medium modifications, leading to a reduced mass shift of pseudoscalar D and vector D^* mesons from their vacuum values. The weak decay constant ratios f_M^*/f_M decreased with increasing baryon density, especially for mesons containing light (u/d) quarks, while mesons having heavier s and c quark pair showed minimal change with rising temperature and isospin asymmetry η . We also analyzed the medium-dependent DAs, $\phi_M^*(x)$, of D and D^* mesons as a function of the longitudinal momentum fraction x . In vacuum, the DAs showed the expected convex-concave structure, indicating that the charm quark carries majority of the meson's momentum. The DAs of vector D^* mesons display higher peaks in comparison to the pseudoscalar D mesons due to contributions from the $2\mathbf{k}_\perp^2/M^*$ term in the wave function. The DA profile for the D_s meson had the lowest peak due to the small mass difference between the c and s quarks. In contrast, for vector mesons, the trend was reversed, with D_s^* displaying a maxima compared to D^{0*} and D^{+*} mesons. At finite ρ_B and η , significant modifications in the DAs were observed. Increasing η from 0 to 0.5 led to a noticeable DA splitting between the D^0 and D^+ mesons for $x < 0.7$, and between D^{0*} and D^{+*} mesons for $x < 0.24$. A slight shift in the maxima towards the left was observed for both pseudoscalar and vector D mesons. Increasing ρ_B from ρ_0 to $3\rho_0$ resulted in DAs of D^0 , D^+ , and their vector coun-

terparts to increase in the region $x > 0.3$, while a suppression was observed at lower x . In contrast, D_s and D_s^* mesons exhibit only a slight decrease in the intermediate $0.3 < x < 0.5$. A change in temperature from $T = 0$ to 0.1 GeV produced no change in the DAs at finite ρ_B , further confirming weak thermal sensitivity.

This work strengthens the link between quark-level dynamics and phenomenological hadronic models probing the internal structure of mesons in dense nuclear environments. It lays a theoretical foundation for understanding the behavior of medium effects on open charm mesons under extreme conditions. The results are particularly relevant for ongoing and upcoming experiments, such as CBM and PANDA at FAIR, where in-medium modifications of charm hadrons may be probed. The framework presented here can be extended to study other non-perturbative QCD phenomena, including in-medium electromagnetic form factors, Mellin moments, and related hadronic observables of heavy mesons in the dense matter.

V. ACKNOWLEDGEMENT

H.D. would like to thank the Science and Engineering Research Board, Anusandhan-National Research Foundation, Government of India under the scheme SERB-POWER Fellowship (Ref No. SPF/2023/000116) for financial support. A. K. sincerely acknowledge Anusandhan National Research Foundation (ANRF), Government of India for funding of the research project under the Science and Engineering Research Board-Core Research Grant (SERB-CRG) scheme (File No. CRG/2023/000557).

VI. REFERENCE

-
- [1] J. J. Aubert *et al.* [European Muon], Phys. Lett. B **123**, 275 (1983).
 - [2] K. Suzuki, M. Fujita, H. Geissel, H. Gilg, A. Gillitzer, R. S. Hayano, S. Hirenzaki, K. Itahashi, M. Iwasaki and P. Kienle, *et al.* Phys. Rev. Lett. **92**, 072302 (2004).
 - [3] E. Friedman, M. Bauer, J. Breitschopf, H. Clement, H. Denz, E. Doroshkevich, A. Erhardt, G. J. Hoffman, R. Meier and G. J. Wagner, *et al.*, Phys. Rev. Lett. **93**, 122302 (2004).
 - [4] F. Bonutti *et al.* [CHAOS], Phys. Rev. Lett. **77**, 603 (1996).

- [5] P. Camerini *et al.* [CHAOS], Nucl. Phys. A **735**, 89 (2004).
- [6] M. F. M. Lutz *et al.* [PANDA], [arXiv:0903.3905 [hep-ex]].
- [7] H. Ohnishi, F. Sakuma and T. Takahashi, Prog. Part. Nucl. Phys. **113**, 103773 (2020).
- [8] S. Sawada, Nucl. Phys. A **782**, 434 (2007).
- [9] T. Sakaguchi [J-PARC-HI], PoS **CORFU2018**, 189 (2019).
- [10] P. Senger, Central Eur. J. Phys. **10**, 1289 (2012).
- [11] V. D. Kekelidze, *et al.*, Phys. Part. Nucl. **48**, 727 (2017).
- [12] V. Kekelidze, *et al.*, Nucl. Phys. A **967**, 884 (2017).
- [13] R. Rapp, D. Blaschke and P. Crochet, Prog. Part. Nucl. Phys. **65**, 209 (2010).
- [14] D. N. Kim and G. A. Miller, Phys. Rev. C **106**, 055202 (2022).
- [15] P. T. P. Hutaaruk, Y. Oh and K. Tsushima, Phys. Rev. C **99**, 015202 (2019)
- [16] C. D. Roberts and S. M. Schmidt, Prog. Part. Nucl. Phys. **45**, S1-S103 (2000).
- [17] J. P. B. C. de Melo, K. Tsushima and I. Ahmed, Phys. Lett. B **766**, 125 (2017).
- [18] J. P. B. C. de Melo and K. Tsushima, Phys. Lett. B **788**, 137 (2019).
- [19] N. Kaur, S. Puhan, R. Pandey, A. Kumar, S. Dutt and H. Dahiya, Phys. Lett. B **859**, 139114 (2024).
- [20] D. Singh, S. Puhan, N. Kaur, M. Kaur, A. Kumar, S. Dutt and H. Dahiya, Phys. Rev. D **111**, 054001 (2025).
- [21] S. Puhan, N. Kaur, A. Kumar, S. Dutt and H. Dahiya, Phys. Rev. D **110**, 054042 (2024).
- [22] S. Puhan, N. Kaur, A. Kumar, S. Dutt and H. Dahiya, Nucl. Phys. B **1017**, 116940 (2025).
- [23] Tanisha, S. Puhan, N. Kaur, A. Kumar and H. Dahiya, [arXiv:2504.21392 [nucl-th]].
- [24] K. Tsushima and J. P. B. C. de Melo, Few Body Syst. **58**, 85 (2017).
- [25] D. Zschesche, A. Mishra, S. Schramm, H. Stoecker and W. Greiner, Phys. Rev. C **70**, 045202 (2004).
- [26] T. Matsui and H. Satz, Phys. Lett. B **178**, 416 (1986).
- [27] M. Gonin *et al.* [NA50], Nucl. Phys. A **610**, 404C (1996)
- [28] C. Garcia-Recio, J. Nieves and L. Tolos, Phys. Lett. B **690**, 369 (2010).
- [29] L. Tolos, Int. J. Mod. Phys. E **22**, 1330027 (2013).
- [30] K. Tsushima, D. H. Lu, G. Krein and A. W. Thomas, Phys. Rev. C **83**, 065208 (2011).
- [31] L. Tolos, J. Schaffner-Bielich and H. Stoecker, Phys. Lett. B **635**, 85 (2006).
- [32] L. Tolos, J. Schaffner-Bielich and A. Mishra, Phys. Rev. C **70**, 025203 (2004)
- [33] M. F. M. Lutz and C. L. Korpa, Phys. Lett. B **633**, 43 (2006).
- [34] W. Cassing, E. L. Bratkovskaya and A. Sibirtsev, Nucl. Phys. A **691**, 753 (2001).

- [35] A. Hayashigaki, Phys. Lett. B **487**, 96 (2000).
- [36] K. Tsushima, D. H. Lu, A. W. Thomas, K. Saito and R. H. Landau, Phys. Rev. C **59**, 2824 (1999).
- [37] A. Mishra and A. Mazumdar, Phys. Rev. C **79**, 024908 (2009).
- [38] A. Kumar and A. Mishra, Eur. Phys. J. A **47**, 164 (2011).
- [39] S. Reddy P., A. Jahan C. S., N. Dhale, A. Mishra and J. Schaffner-Bielich, Phys. Rev. C **97**, 065208 (2018).
- [40] R. Kumar and A. Kumar, Phys. Rev. C **101**, 015202 (2020).
- [41] R. Chhabra and A. Kumar, Phys. Rev. C **98**, 025205 (2018).
- [42] R. Chhabra and A. Kumar, Eur. Phys. J. A **53**, 105 (2017).
- [43] A. Kumar, Adv. High Energy Phys. **2014**, 549726 (2014).
- [44] A. Kumar and R. Chhabra, Phys. Rev. C **92**, 035208 (2015).
- [45] A. Hosaka, T. Hyodo, K. Sudoh, Y. Yamaguchi and S. Yasui, Prog. Part. Nucl. Phys. **96**, 88 (2017).
- [46] R. Chhabra and A. Kumar, Springer Proc. Phys. **203**, 657 (2018).
- [47] R. Chhabra and A. Kumar, Eur. Phys. J. C **77**, 726 (2017).
- [48] A. J. Arifi, L. Happ, S. Ohno and M. Oka, Phys. Rev. D **110**, 014020 (2024).
- [49] A. J. Arifi, P. T. P. Hutaaruk and K. Tsushima, Phys. Rev. D **107**, 114010 (2023).
- [50] S. J. Brodsky, H. C. Pauli and S. S. Pinsky, Phys. Rept. **301**, 299 (1998).
- [51] K. G. Wilson, T. S. Walhout, A. Harindranath, W. M. Zhang, R. J. Perry and S. D. Glazek, Phys. Rev. D **49**, 6720 (1994).
- [52] P. Wang, Z. Y. Zhang and Y. W. Yu, Commun. Theor. Phys. **36**, 71 (2001).
- [53] R. Kumar and A. Kumar, Eur. Phys. J. C **79**, 403 (2019).
- [54] P. Papazoglou, D. Zschesche, S. Schramm, J. Schaffner-Bielich, H. Stoecker and W. Greiner, Phys. Rev. C **59**, 411 (1999).
- [55] A. Kumar and A. Mishra, Phys. Rev. C **82**, 045207 (2010).
- [56] H. Singh, A. Kumar and H. Dahiya, Chin. Phys. C **41**, 094104 (2017).
- [57] P. Wang, Z. Y. Zhang, Y. W. Yu, R. K. Su and Q. Song, Nucl. Phys. A **688**, 791 (2001).
- [58] P. Wang, Z. Y. Zhang, Y. W. Yu, H. Guo, R. K. Su and H. Q. Song, Nucl. Phys. A **705**, 455 (2002).
- [59] A. Kumar, S. Dutt and H. Dahiya, Eur. Phys. J. A **60**, 4 (2024).
- [60] N. Barik, B. K. Dash and M. Das, Phys. Rev. D **31**, 1652 (1985).
- [61] N. Barik, R. N. Mishra, D. K. Mohanty, P. K. Panda and T. Frederico, Phys. Rev. C **88**, 015206 (2013).
- [62] B. D. Keister and W. N. Polyzou, Adv. Nucl. Phys. **20**, 225 (1991).

- [63] H. M. Choi and C. R. Ji, Phys. Rev. D **59**, 074015 (1999).
- [64] H. M. Choi and C. R. Ji, Phys. Rev. D **80**, 054016 (2009).
- [65] H. M. Choi and C. R. Ji, Phys. Lett. B **460**, 461 (1999).
- [66] A. J. Arifi, H. M. Choi, C. R. Ji and Y. Oh, Phys. Rev. D **106**, 014009 (2022).
- [67] H. M. Choi, C. R. Ji, Z. Li and H. Y. Ryu, Phys. Rev. C **92**, 055203 (2015).
- [68] S. Navas *et al.* [Particle Data Group], Phys. Rev. D **110**, 030001 (2024).
- [69] N. Dhiman, H. Dahiya, C. R. Ji and H. M. Choi, Phys. Rev. D **100**, 014026 (2019).
- [70] Z. G. Wang, Eur. Phys. J. C **75**, 427 (2015).
- [71] D. Becirevic, P. Boucaud, J. P. Leroy, V. Lubicz, G. Martinelli, F. Mescia and F. Rapuano, Phys. Rev. D **60**, 074501 (1999).
- [72] G. Cvetic, C. S. Kim, G. L. Wang and W. Namgung, Phys. Lett. B **596**, 84 (2004).
- [73] G. L. Wang, Phys. Lett. B **633**, 492 (2006).
- [74] T. Hilger, R. Thomas and B. Kampfer, Phys. Rev. C **79**, 025202 (2009).
- [75] H. M. Choi, Phys. Rev. D **75**, 073016 (2007).
- [76] Z. G. Wang, Phys. Rev. C **92**, 065205 (2015).
- [77] V. L. Chernyak and A. R. Zhitnitsky, Phys. Rept. **112**, 173 (1984).
- [78] G. P. Lepage and S. J. Brodsky, Phys. Rev. D **22**, 2157 (1980).
- [79] H. M. Choi and C. R. Ji, Phys. Rev. D **75**, 034019 (2007).
- [80] Y. Li, P. Maris and J. P. Vary, Phys. Rev. D **96**, 016022 (2017).
- [81] T. Zhong, K. Li, Y. Zhang and H. B. Fu, Int. J. Theor. Phys. **59**, 2562-2571 (2020).
- [82] Y. Zhang, T. Zhong, H. B. Fu, W. Cheng and X. G. Wu, Phys. Rev. D **103**, 114024 (2021).
- [83] F. E. Serna, R. C. da Silveira, J. J. Cobos-Martínez, B. El-Bennich and E. Rojas, Eur. Phys. J. C **80**, 955 (2020).